Master's Thesis

Analyzing V2V signal models in simulated 3D geometry-based stochastic channels

By

Hussam Mohamed
And
Darshan Manjunath Rao Chawan

Department of Electrical and Information Technology
Faculty of Engineering, LTH, Lund University
SE-221 00 Lund, Sweden

Abstract

Vehicle to everything (V2x) communication is one of the most researched topics today. The main goal behind this new emerging technology is road safety along with traffic and energy efficiency. Vehicular communications can further be sub-divided into certain types. One such type is vehicle to vehicle (V2V) communication, which is the focus of this thesis. V2V is either Wireless Local Area Network (WLAN) based or cellular based. In order to analyze and enhance this technology, real measurements need to be performed, which further require the use of different signal models.

For the thesis, the V2x WLAN based signal model has been used. This involved use of a V2x simulator for various stochastic channels and for a site-specific channel. The thesis is divided into three parts. The first part involves the building of a deterministic V2V channel model in the Unity 3D game engine. This deterministic channel is simulated by mimicking the 3D geographical properties of the Faculty of Engineering (LTH) premises of Lund University. The second part of the thesis is about understanding the V2x simulator. Further, the tasks involved analyzation of IEEE 802.11p and next generation 802.11bd protocols performance in stochastic channels. These stochastic channels were created using real-time measurements in ublox company. The final part of the project involves the use of the V2x simulator to assess the created V2V channel model. The proposed solution was to merge the deterministic channel to the simulator model. This was achieved by mixing the stochastic approach with our deterministic channel and then analyzing the performance. The results show that IEEE signal models in simulated line of sight (LOS) environment and in a stochastic LOS environment behave similarly.

Acknowledgments

Table of Contents

Preface

This thesis work is done by the jointly contribution of two students (Hussam and Darshan). The individual contributions in the main parts of the research and writing is mentioned in the table below:

	Sections	**Contributions**
Chapter 1	Background Objective and aim Report structure	Darshan Hussam Darshan
Chapter 2	V2x Signal models Channel model & properties	Darshan Darshan Hussam
Chapter 3	Channel model Channel impulse response V2x simulator model	Hussam Hussam & Darshan Hussam
Chapter 4	Channel model results V2x simulator model	Hussam & Darshan Hussam
Chapter 5	Conclusions Future work	Hussam Hussam

Popular Science Summary

Since the development of vehicles, our life has become easier. But every positive value has its price in negative terms. With the increase in the car population, the accidents occurring from vehicles increased. Hence, there was a need to find a way to minimize accidents as much as possible, that is why the vehicular communication system was developed. A system is composed in a term called vehicular to everything (V2x), in which vehicles can communicate with each other or with other entities that may affect the vehicle. Therefore, by using V2x communication the number of accidents can be significantly reduced.

In the future, V2x communication will be implemented in a wide range of cars. Using V2x communications makes vehicles respond to any situation with a delay much lesser than of the average human's time to respond to any situation while driving. For instance, if the driver of a car in front suddenly pushed the breaks in a high way, the vehicles behind with a V2x technology will respond immediately before the driver's mind analyze the situation.

To measure and analyze the performance of the vehicle to vehicle communications (V2V), real-time measurements can be done using the various WLAN signal models (IEEE802.11p and IEEE802.11bd) of V2x. In this thesis project, analyzation of the performance of the WLAN signal models on different real-time stochastic channels is done by using the V2x simulator. A V2V channel model is simulated between two cars in a realistic 3D environment extracted from Google Earth. The latter is done to test the performance of the WLAN signal models on these types of deterministic channels. Hence, instead of doing real-time measurements, simulated channels can be used to measure and enhance the performance of V2x signal models. Lastly, a comparison between the performance of the WLAN signal model and the next-generation model was done on the simulated channel and on the stochastic channels. The performance of these signal models on the simulated 3D channel was noticed to behave similarly to the performance of the same IEEE signal models on one of the real-time stochastic channel scenarios.

CHAPTER 1

Introduction

This chapter gives a detailed description of the background behind this thesis work. Then the main objectives and aim of the thesis, and then the chapter is finalized with how the report is structured.

1.1 Background

V2x, which means 'vehicle to everything', is an umbrella term for the vehicle's correspondence framework, where data from sensors and different sources voyages through high-bandwidth, low-inactivity, high-reliability links, making ready to completely self-sufficient driving. There are a few parts of V2x, including vehicle-to-vehicle (V2V), vehicle-to-Infrastructure (V2I), vehicle-to-pedestrian (V2P), and vehicle-to-network (V2N).

3GPP is moving towards enhancing the V2x communication, while on the other hand IEEE 802.11 group is moving towards the next generation V2x (NGV) at the same time [2]. It is clear by the fact what NGV 802.11bd will add to the previous standard 802.11p in V2V communication. One of the major differences between the previous standards and the NGV, is the channel estimation. It is done by sending a training sequence that is known by the receiver (pilots). The receiver can then estimate the channel impulse response by comparing the received data [3], [7]. The preamble, pilots added in front of the packet, is used for packet detection and channel estimation in time-invariant channels. But using preambles for time-variant channels due to user mobility will cause error in the progress of compensation and the performance will degrade. That is why we need mid-ambles to keep track and acquire a more accurate estimation [3].

1.2 Objective and aim

The aim of this Master's thesis work is to simulate a 3D vehicular communication channel model in Unity 3D, which is a game engine for developing games, using ray tracing and a real geographical

environment. After creating the channel model, we analyze the IEEE 802.11p signal model on the designed channel model and then compare it with the next generation signal model IEEE 802.11bd. Lastly, we compare the performance of the simulated channel model with the stochastic channel models. These stochastic channel models are modeled by Ioannis Sarris and Sebastian Schiessl from ublox company, Athens using real-time measurements through the ublox-V2x simulator.

1.3   Report structure

The rest of this thesis is organized in the following way. Chapter 2 explains the theory of V2x communications, IEEE 802.11p, Dedicated Short Range Communication (DSRC), IEEE 802.11bd and the channel model properties such as Line of Sight (LOS), non-Line of Sight (non-LOS), Reflection, Doppler shift etc. Chapter 3 explains the methodology of building the ublox-V2x simulator. The methodology is performed by simulating a 3D environment in Unity 3D, and the results of multipath propagation in Unity 3D are simulated in the ublox-V2x simulator. To check the simulated channel model, an approach is performed by considering theoretical values of IEEE 802.11p and by determining channel impulse response whose power and amplitude values are extracted from Unity 3D model and then this approach is compared with the two-ray-ground-reflection model approach. Chapter 4 shows the simulation results of this thesis work. The results include Unity 3D channel model results and ublox-V2x simulator results. Finally, Chapter 5 summarizes and concludes this thesis work and it further suggests several ideas as future work for V2x simulation model.

CHAPTER 2

Theory

This chapter is about the theory used in the research. It includes a thorough description of V2x, IEEE signal models and the channel model, including the channel properties and theories used to build that model.

2.1 V2x communication

In 2010, the IEEE 802.11p V2x standard was introduced for wireless local area networks (WLAN) [7]. Using the DSRC, information exchange is done between the networks without the help of a basic service set (BSS), which is required in 802.11 standards [10]. After the inclusion of massive Multiple Input Multiple Output antenna systems (MIMO), Low Density Parity Check (LDPC) codes, and certainly better handling Doppler shifts, V2x has evolved as one of the developed technologies in 802.11bd standard. For 802.11bd standard, a study group created 'NGV-V2x' for wireless Local Area Network (LAN) technologies [10].

Vehicular communications with the help of connected cars and roadside units have given a rapid potential to reduce the number of accidents, through sharing information with each other they help in vehicle safety [10]. A number of studies were performed to evaluate their performance in various scenarios such as Cellular V2x (C-V2x), New Radio-V2x (NR-V2x), IEEE802.11p V2x, and IEEE802.11bd-V2x communications. During the Rel. 14, Third-generation Partnership Project (3GPP) developed C-V2x which benefits the cellular infrastructure [7]. Since C-V2x cannot depend always on the cellular infrastructure, various modes of transmission are formed such as side link channel with PC5 interface to communicate directly with V2x communications [7]. PC5 is a reference point where User Equipment (UE) can communicate with another UE without a base station [7]. Discrete Fourier Transform (DFT) spread Orthogonal Frequency Division Multiplexing (OFDM) technique is used in C-V2x to increase power efficiency [10]. It has a 10 times larger symbol duration when compared to 802.11p which results in reduced Inter Symbol Interference

(ISI) and provides robustness against multipath propagation and fading [10]. In the case of 5G NR-V2x communications, both OFDM and DFT spread OFDM are used for uplink transmission [10]. During the Release.16, 3GPP has finalized specifications for Fifth Generation (5G) NR-V2x communications which is mainly concentrated on the uplink transmission. IEEE 802.11p/Intelligent Transport Systems Generation 5 (ITS-G5) based V2x communications have made an encouraging effort to bring better road safety and traffic efficiency applications [12]. With a small delay, data is exchanged between the vehicles via the roadside units. Similar specifications of 802.11p V2x communications apply to 802.11bd, but here in 802.11bd there is an increase in the speed of vehicles (500kmph), and also the number of subcarriers which are allocated for data are 56 which are useful subcarriers [12]

The position and movement of a vehicle can be detected up to a quarter kilometer away by using "V2V communication". Using a simple antenna, a computer chip, and Global Positioning System (GPS), vehicles can be tracked even though they are at blind spots, hidden in highway, or even blocked by other vehicles [29]. They instantly warn the drivers with emergency warning messages, when the vehicles are about to change the driving situations (Speed, sudden break). When two or more vehicles are within a radio communication range, they connect automatically and forms an ad hoc network [29]. For V2V communications, for safety purpose a Collision Detection Algorithm for Intersections (CDAI) is inserted on each vehicle to obtain information among vehicles which are approaching, leaving, and crossing the intersection [28]. These algorithms use vehicle's path prediction and determines space conflicts whenever the vehicle crosses the intersection. These intersections are considered as a polygon on each lane on the road from the previous intersection to the next upcoming intersection. From the current road segment, current lane, and next road segment, CDAI anticipates the path taken by vehicle to cross the intersection and forms two polygons, one of them is regarded as the current road segment among two intersections and the other one is for next road segment [28]. So, these two polygons are referred to as Trajectory Box (TB). To determine the intersection of TB's between two vehicles, a 'Separating Axis theorem' is used [10]. This theorem explains that "a pair of convex polygons which are not in the same state of collision, and they are perpendicular to one edge of the polygon axis, and between the projected surfaces of two polygons there will not be any overlap".

Several challenges which we face in IEEE 802.11bd V2x communications are interoperability and backward compatibility requirements [10]. These

two are major critical requirements for 802.11bd. 802.11bd devices will only be able to communicate with other 802.11bd devices without Interoperability. By illustrating using multiple antenna schemes such as space-time block coding or by use of alternative wave-forms may violate the Interoperability requirements in Medium Access Control (MAC) and Physical (PHY) layers of 802.11bd [10].

With minimum latency, the intelligence insight the transport systems must make the traffic information available for all the users, thereby the chances of accidents can be reduced [27]. After the implementation of V2x, the road deaths statistics has been reduced in the European Union (EU) by 57.5% between 2001 and 2017. Most of the accidents occur in traffic roads and urban areas due to poor visibility, difficult to see obstacles, and mixed traffic [27]. Hence, V2x has a reliable non-line of sight (NLOS) sensor that works in all the environments and even in the worst weather conditions by sending alert messages to the drivers which also help to reduced accidents and improve road safety in the modern-day environment.

2.2   Signal models

In V2x communications, there are two types of signal models used. One is the IEEE 802.11p model and the other is the next generation model which is called IEEE 802.11bd.

2.2.1   IEEE 802.11p

The Institute of Electrical and Electronics standard (IEEE 802.11 std) has developed an amendment which is known as 'IEEE 802.11p' for Vehicular Environment. For vehicle's safety, traffic speed up, digital map update in vehicles and other such applications, this amendment has been implemented [1]. To address all these concerns, 802.11p formed a document which is known as 'Wireless Access in Vehicular Environment' (WAVE) [1]. WAVE standardization basically originated from DSRC. DSRC communications are the wireless communication channels which are designed for automotive use to make them communicate one way or two way between short range to medium range communication channels. This DSRC communication channel has 75 MHz of spectrum bandwidth in the United States (U.S) with an allocated frequency between 5.85-5.92 GHz which has been used for

V2V, V2I communications [1]. The Binary Convolution Coding (BCC) technique is used in 802.11p standard for error correction [3].

The basic idea for implementing IEEE 802.11 standard for WAVE is due to availability of WAVE standard in all the parts of the world which also includes the U.S [1]. 802.11p uses either 10 MHz or 20MHz of channel bandwidth. For the 10 MHz channel bandwidth, it has subcarrier spacing of 0.15 MHz. So, within this sub-carrier spacing, there are 64 sub-carriers in which 52 subcarriers are used for data transmission that are also further composed of 48 sub-carriers with 4 pilot sub-carriers [1]. The parameters for implementing 802.11p is shown in table 2.1 [3].

Parameters	
Bit rate (Mb/s)	3, 4, 5, 6, 9, 12, 18, 24, 27
Modulation mode	BPSK,QPSK,16QAM,64QAM
Number of sub-carriers	52
Subcarrier spacing	0.15625 MHz
Code rate	1/2, 2/3, 3/4
Guard time	1.6 µs
FFT period	6.4 µs

Table 2.1: PHYs implementation in IEEE 802.11p [3]

Here in 802.11p, the 48 data sub-carriers can be modulated using different modulation techniques such as Binary Phase Shift Keying (BPSK), Quadrature Phase Shift Keying (QPSK), Quadrature Amplitude Modulation (QAM) with the constellation size of 16 (16-QAM) or 64QAM, with different coding rates [3]. Figure 2.1 shows the frame format of IEEE 802.11p standard. It consists of OFDM Physical Layer Convergence Protocol (PLCP) preamble is used for initial channel estimation of data symbols and PLCP preamble consists of 10 identical short training symbols and 2 identical long training symbols, PLCP header is always transmitted at 1Mbps and to decode the frame structure, the PLCP header carries some logical information, PLCP Service Data Unit (PSDU), tail bits and pad bits [1].

6

PLCP is a convergence process that shifts the Packet Data Unit (PDU) coming from the MAC layer to form an OFDM frame. This process is always responsible for communication with the MAC layer to send packets of data units to form an OFDM frame [3].
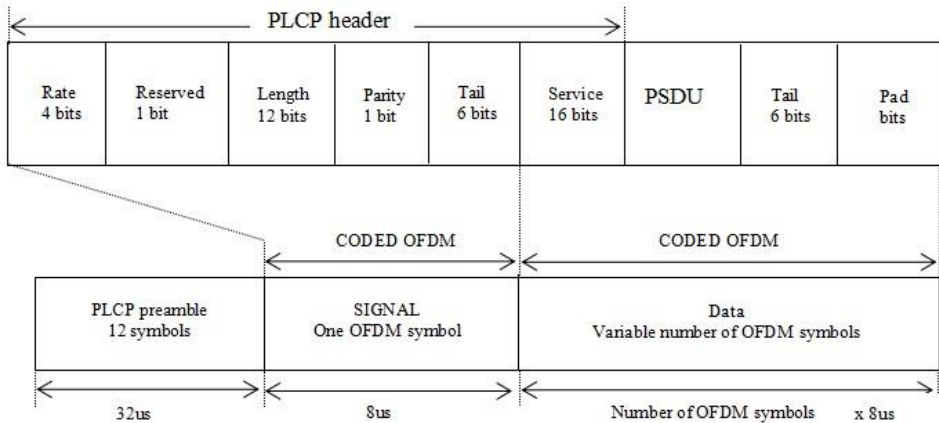

Figure 2.1: Frame format of IEEE 802.11p

2.2.1.1 Dedicated short range communications

DSRC is basically defined from PHY and MAC layers of 802.11p standard, which is largely derived from 802.11a standard [7]. These are extensively studied using analytical models, extensive simulation studies, and field trials [7]. With frequency band of 5.9 GHz, DSRC are basically designed in radio access technologies (RATs). DSRC were intended for vehicular systems portrayed by high-mobility, thereby improvements were made to make DSRC appropriate for such situations. Subcarrier spacing in DSRC is reduced by a factor of two, since it uses OFDM as a PHY layer with a channel bandwidth of 10 MHz [7]. Communication between nearby vehicles and road-side units is performed efficiently using DSRC technique.

Carrier Sense Multiple Access (CSMA) is one of the MAC protocols used in DSRC [7]. The parameter dispute window that is utilized in conflict based MAC conventions stays fixed in DSRC, because of two primary reasons, one reason is the fact that DSRC is structured for communication based frameworks in which no affirmation outline is sent back to the transmitter,

and the second reason is the exponential back-off can prompt enormous dispute window sizes, in this manner prompting high latencies.

2.2.2   IEEE 802.11bd

The main specifications of IEEE 802.11bd have been formed from 802.11 task group (TGbd) [10]. 802.11bd has relative velocity speed up of 500km/hour [7]. Decoding of at least one mode of transmission is done for 802.11p by 802.11bd protocol and contrariwise, which shows the interoperability between both of the protocols [7]. Equal channel access opportunities must be given between both (802.11p and 802.11bd) protocols for the fairness of the channel. Due to high reliability, the packet collisions and the higher Doppler shifts can be reduced in 802.11bd [10]. Using LDPC, MIMO, and 256 QAM modulation the high data rate can be achieved in 802.11bd protocol. The physical parameters for implementing 802.11bd is shown in table 2.2[11] [3].

Feature	
Radio bands of operation	5.9 GHz & 60 GHz
Channel coding	LDPC
Doppler recovery method	High frequency midambles
Sub-carrier spacing	312.5 KHz, 156.25 KHz, 78.125 KHz
Supported relative speeds	500 Kmph
FFT size	56 sub carriers
Channel bandwidth	10 MHz/20 MHz

Table 2.2: PHYs implementations in IEEE 802.11bd [3], [11]

By proposing diversities such as Space time block coding (STBC) or Data Communication module (DCM), the reliability of 802.11bd standard can be increased [11]. STBC enables two signal branches on the transmitter side

whereas the frequency diversity-based DCM utilizes two signal branches from STBC [11]. In order to make 802.11 standards more suitable for outdoor environments, the Multiple Cyclic prefix (CP) is used to avoid ISI [10]. For transmission latency calculations in 802.11bd, a 4µs header for normal packet, and 8µs packet for extended range are considered [10].The PHY of 802.11bd is designed by using PHY of 802.11ac as a base-line and half the Subcarrier spacing (known as ''2 x down-clock''), which means that the 64 sub carriers can be fixed in 802.11bd for a 10 MHz channel bandwidth. For 802.11p the same approach can be done by using PHY of 802.11a and by reducing the sub-carrier spacing by a factor of two [7]. But while comparing 802.11a and 802.11ac, the 802.11ac performs better by using 2xdown-clock with LDPC coding. Hence, by using LDPC coding 802.11bd becomes more efficient when compared to 802 .11p. Midambles are used in 802.11bd to increase channel estimation accuracy [7].
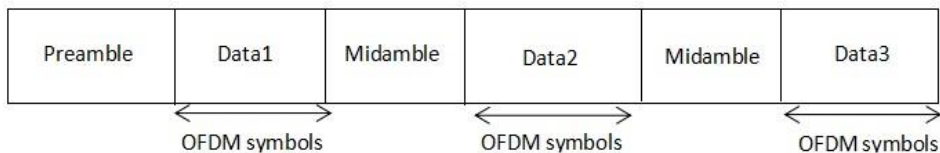

Figure 2.2: Midambles insertion for improved Channel Estimation

The preamble in Figure 2.2 is used for synchronization and channel estimation in the beginning of the frame. The same preamble can't be used later in the frame, the initial channel estimate becomes outdated since the channel is varying fast and there are chances of erroneous reception if we use the same preamble for the channel estimation [7]. Hence, the preamble is only available until Data1 in figure 2.2.

For further channel tracking in the frame, the high frequency midambles are used between the OFDM data symbols, so that specific channel estimation is performed for the remaining data symbols [7]. Added to that, the midambles are inserted for every 9th OFDM symbol modulation coding scheme (MCS) from MCS0 to MCS4, and alternatively (extended cyclic prefix) for every 4th OFDM symbol [10]. 802.11bd is more reliable with improved range and throughput when compared to 802.11p [10].

2.2.3 Comparison between 802.11p and 802.11bd

Table below shows the key mechanisms between 802.11p and 802.11bd standard [7].

Feature	802.11p	802.11bd
Radio bands of operation	5.9 GHz	5.9 GHz – 60Gz
Channel coding	BCC	LDPC
Re-transmissions	None	Congestion dependent
Counter measures against Doppler shift	None	Midambles
Sub-carrier spacing	156.25 KHz	156.25KHz, 312.5 KHz, 78.125 KHz
Relative speeds	252 Km/h	500 Km/h
Spatial streams	One	multiple

Table 2.3: 802.11p and 802.11bd comparison

2.3 *Channel model and properties*

2.3.1 Wireless channel properties

A wireless channel is the medium of propagation between the transmitter and the receiver. Wireless channels differ from wired channels, since the wireless channels are affected by multipath propagation phenomena, which means that the signal transmitted from the transmitter, have several paths to reach the receiver. These paths can occur due to reflections, diffractions, diffuse scattering or even the direct path from transmitter to the receiver. The latter path is called Line of Sight (LOS) while others are called non-Line of Sight (non-LOS) paths. [13]

2.3.1.1 Line of sight

Assuming that the transmitter and receiver are in free space, Friis' law indicates that the received power P_{RX} at the receiver will be attenuated with the increase of the carrier frequency f or distance d as shown in equation 2.1 [13],

$$P_{RX} = P_{TX}\, G_{TX} G_{RX} \left(\frac{c}{4\pi df}\right)^2 . \qquad\qquad 2.1$$

Here P_{TX} is the transmitted power, G_{TX} and G_{RX} are the antenna gains of the transmitter and the receiver respectively [13]. The speed of light c is $3 \times 10^8\, m/sec$.

Power in decibels (dB) is more convenient in the telecommunication field since the power is always measured as a ratio, and dB scale gives that measure in a logarithmic scale. Friis' equation in dB is shown below in equation 2.2,

$$P_{RX\_dB} = P_{TX\_dB} + G_{TX\_dB} + G_{RX\_dB} \qquad\qquad 2.2$$
$$+ 20\, log\left(\frac{c}{4\pi df}\right).$$

Friis' law is restricted to the far field i.e. the transmitter (TX) and the receiver (RX) should be separated by at least one Rayleigh distance [13]. Rayleigh distance d_r is defined as in equation 2.3 where L_a is the largest dimension of the antenna,

$$d_r = \frac{2fL_a{}^2}{c} . \qquad\qquad 2.3$$

By assuming isotropic antennas on both TX and RX ($G_{TX} = G_{RX} = 1$), the attenuation of the LOS signal depends massively on the wave length ($\lambda = \frac{c}{f}$) and the distance. This attenuation is inverse of the Free Space Loss Factor (FSLF). Equation 2.4 and Figure 2.3 demonstrate the dependency,

$$FSLF = \left(\frac{\lambda}{4\pi d}\right)^2.$$
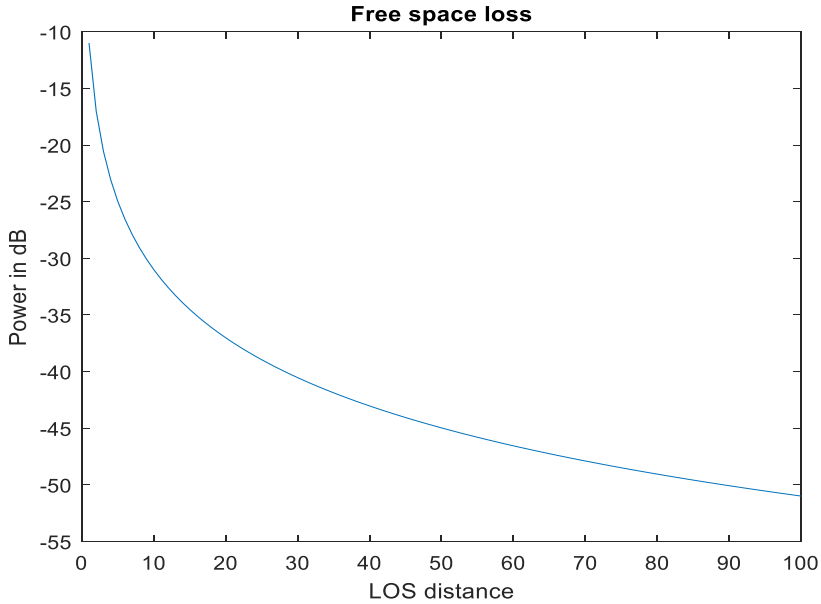<div align="right">2.4</div>

Figure 2.3: Free space loss in dB vs Distances in meters

2.3.1.2 Non line of sight

In a real-time environment, most of the time there will be dielectric and conducting objects between the TX and RX. These objects affect the channel by adding non-LOS paths. If these objects have smooth surfaces, the signal will reflect, whereas if the surface is rough, the signal will scatter in different directions. Added to that, electromagnetic waves (signals) can also get diffracted at the edges of these objects [13].

2.3.1.3 Reflection

Reflection occurs when the specular ray hits a smooth surface. Since electromagnetic waves behave in the same fashion as the specular ones (especially in high carrier frequencies), their reflection is approximately the same on smooth surfaces. In such cases, the angle of incidence (ψ) is the same as the angle of reflection (ψ) according to Snell's law [13].

The reflection coefficient along with the direction of reflection determines the power that arrives at the RX. Using the two-ray ground reflection model, we can find the reflection coefficient [15].
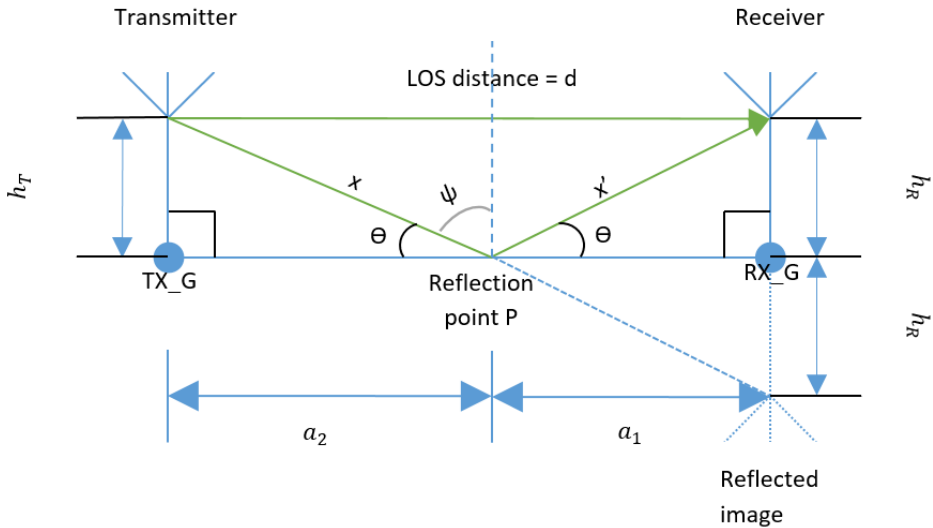
Figure 2.4: two-ray model

Figure 2.4 shows the two-ray ground model reflection. The received power on the LOS path will be the same as equation 2.2, however the ground (or any other material) reflected power will be as:

$$P_{ref} = P_{TX} \cdot \alpha(\Theta) \cdot G_{TX} \cdot G_{RX} \cdot \left(\frac{c}{4\pi(x+x')f}\right)^2 . \qquad 2.5$$

Where x is the distance from the transmitter to the reflection point, x' is the distance from the reflection point to the receiver and $\alpha(\Theta)$ is the reflection coefficient, which depends on the angle of incidence and the material's properties,

$$\alpha(\Theta) = \frac{\sin\Theta - X}{\sin\Theta + X}.$$ 2.6

In Equation 2.6, X includes the material properties that caused the reflection and depends on the signal polarization. X is described as X_v if the signal is vertically polarized and X_h when the signal is horizontally polarized as shown in equation 2.7,

$$X_v = \frac{X_h}{\varepsilon} = \frac{\sqrt{\varepsilon - \cos^2\Theta}}{\varepsilon}.$$ 2.7

The relative permittivity of the material is ε. Figure 2.5 shows the reflection coefficient for both horizontal and vertical polarization with the change of the angle of incidence Θ.
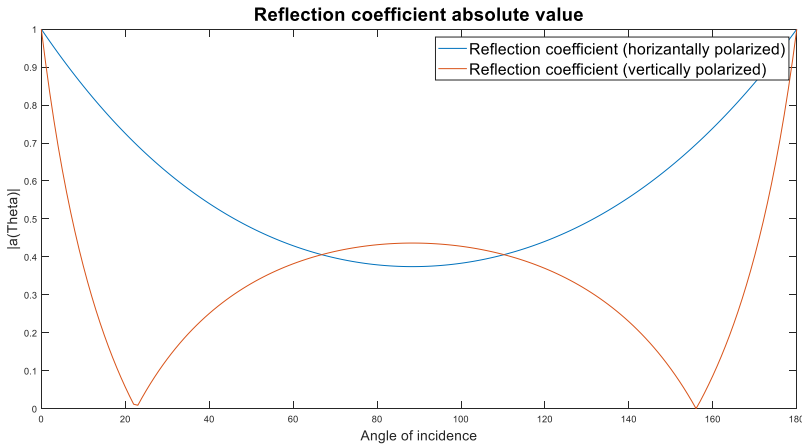
Figure 2.5: Reflection coefficient

2.3.1.3.1 Reflection point algorithm

To find the location of the reflection point P in a three-dimensional environment (3D) some vectors calculations should be done. From Figure 2.4 we can see that the triangle between the Transmitter position, TX_G and P positions is equal to the triangle between Receiver position, RX_G and P. The equality of triangles comes from the fact that their angles are equal. From the equality we can find that:

$$\tan \theta = \frac{h_T}{h_R} = \frac{a_2}{a_1}.$$

2.8

The unit vector $\vec{V}$, which is a vector of length 1 directed from the Transmitter ground position (TX_G) to the Receiver ground position (RX_G), is calculated as in equation 2.9. To find the point of reflection, equations (2.8, 2.9, 2.10 and 2.11) can be used from geographical properties and vectors theory,

$$\vec{V} = \frac{RX\_G - TX\_G}{\|RX\_G - TX\_G\|}.$$

2.9

From Figure 2.4 it can be seen that the distance between TX_G and RX_G is:

$$a_1 + a_2 = \|RX\_G - TX\_G\|.$$

2.10

By solving equation 2.8 and 2.10, values of a_1 and a_2 can be found. Then, since we know that the vector between the reflection point and RX_G (P-RX_G) is the same as the scalar distance multiplied with the unit vector ($\vec{V}$) on the same direction of vector (P- RX_G). Hence, we can get the reflection point as equation 2.11 shows,

$$P = RX_G + \vec{V} . a_1.$$

2.11

2.3.1.4 Diffraction

All of the objects that are in reality, which are in the communication medium, have limited size. Due to the finite size of these intermediate objects and the electromagnetic wave nature, diffraction occurs at the edges of these objects [13]. According to the latter there will not be a complete shadow if an object is replaced between TX and RX, however there will be a portion of the LOS power received in the receiver side as seen in Figure 2.6.
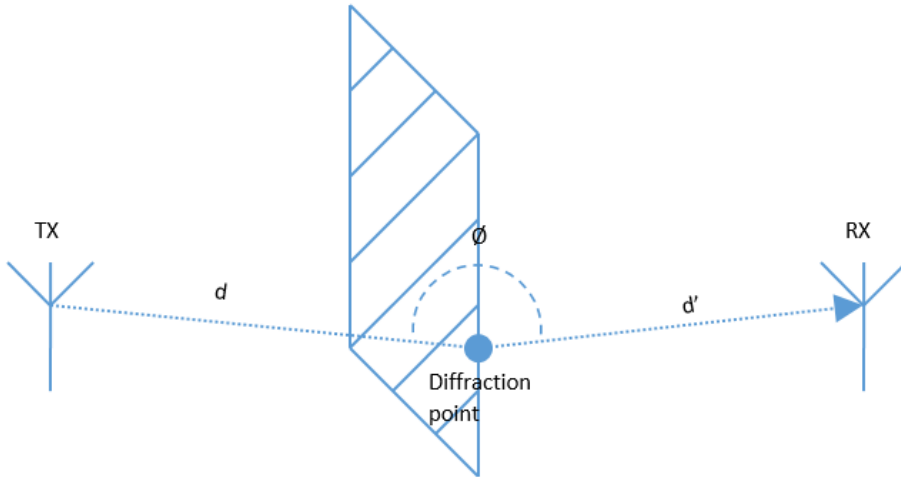

Figure 2.6: Diffraction

The diffraction coefficient β, which effects the power received in the receiver, is dependent on the angle Ø in degrees. The simplest way to calculate this coefficient is equation 2.12,

$$\beta = \frac{\cos(y) + 1}{2}. \qquad\qquad 2.12$$

Where: $y = 180^0$ at $0 < Ø < 165$,
$\quad y = -\frac{180}{13} (Ø - 180)^o$ at $165 < Ø < 180$,
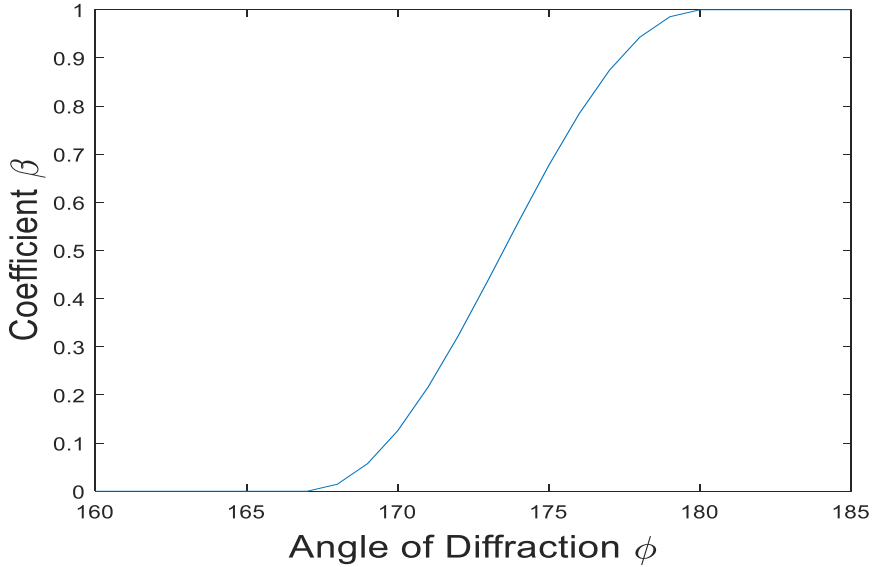$\quad y = 0^0,$ $Ø \geq 180$

Figure 2.7: Diffraction coefficient

According to Figure 2.7 above, if the transmitter is moving and the angle of diffraction is getting bigger, we almost receive the same power as the LOS. In the other hand we get more shadows (no received signal) if the angle is getting smaller. Hence, we receive a portion of the signal when the angle is approximately between (180-167) degrees.

2.3.1.5 Doppler shift

Doppler shifts occur when there is a movement on either the transmitter TX, the receiver RX or both. The movement causes the received frequency to change slightly. Even though the latter change is small (especially when the carrier frequency is very high), the Doppler shift is an important parameter of the channel. Therefore, the Doppler shifts when arriving from multiple components can affect the channel rapidly by making it frequency selective, and this has a high impact on V2x communications. The Doppler frequency shift f_D can be calculated as:

17

$$f_D = \pm \frac{|v|}{\lambda} \cos(\Theta) . \qquad\qquad 2.13$$

Where λ is the wave length $\left(\frac{c}{f}\right)$, v is the TX speed in the direction of wave propagation $v = |v| \cos(\Theta)$ as can be seen in Figure 2.8.
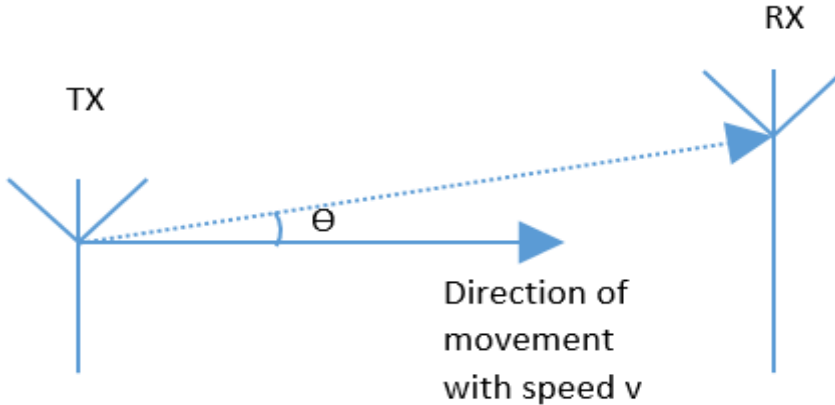

Figure 2.8: Doppler shift

The total received frequency will be:

$$f_{total} = f + f_D. \qquad\qquad 2.14$$

Note that the Doppler frequency is positive when TX and RX are moving towards each other, and negative when the TX or RX is moving away from the other.

With the information from the previous sections, the LOS and non-LOS channel components, R_{LOS} and $R_{non-LOS}$ respectively, at the receiver part can be calculated as:

18

$$R_{LOS} = \frac{c}{4\pi f_{total}} \cdot \frac{exp(-j2\pi dc/f_{total})}{d} . \qquad 2.15$$

$$R_{non-LOS}$$
$$= \frac{c}{4\pi f_{total}} \cdot \alpha(\Theta). \beta \cdot \frac{exp(-j2\pi(x + x')c/f_{total})}{x + x'} . \qquad 2.16$$

2.3.2   Channel statistical properties

The theory described above is useful for a simple environment with one or two multipath components (MPC). These MPC cause reflection, diffraction and scattering. In a real environment, with many MPC, it is more complicated to describe all the processes individually. Hence, it is more convenient to consider the probability that the channel parameters attain a certain value.
At small distances between TX and RX, and with MPC in that environment, the power received at RX fluctuates around a certain mean value. This fluctuation is called small-scale fading that is mainly caused by MPC, adding either destructive or constructive interference [13]. Other fluctuations that appear on larger scale around a certain mean value, is called the large-scale fading. The latter is caused by the objects obstructing the LOS path and is related to the free space loss.

2.3.2.1 Small scale fading without a dominant component

Measurements and experiments done in an environment with a TX, RX and MPC, without a direct LOS between TX and RX, showed that the probability density function (pdf) of the received amplitude and phase, behaves the same way as the Rayleigh distribution. A Rayleigh distribution, shown in Figure 2.9, describes the magnitude of a complex stochastic variable with an independent and normally distributed real and imaginary parts.
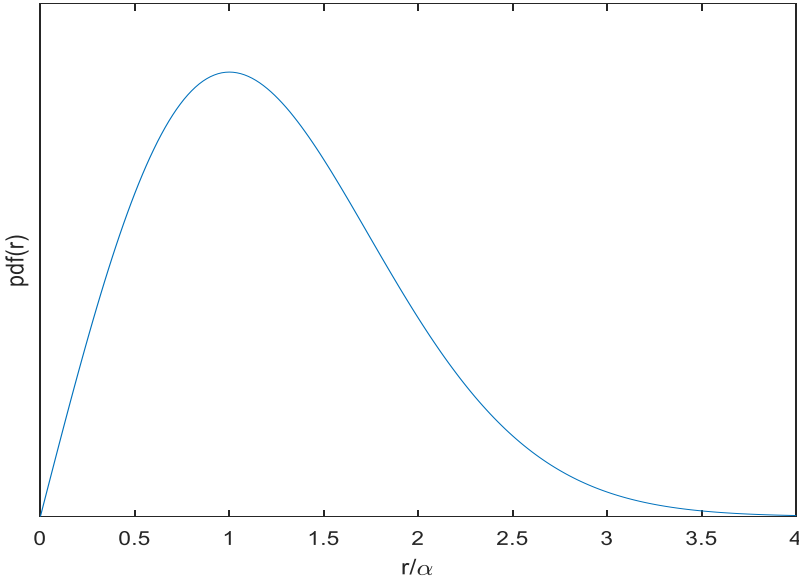
Figure 2.9: Rayleigh distribution

A normally distributed variable x with a zero mean has the pdf:

$$pdf_x(x) = \frac{1}{\sqrt{2\pi}\sigma} exp\left(-\frac{x^2}{2\sigma^2}\right). \qquad 2.17$$

Where σ^2 is the variance of the normal (Gaussian) distribution.
The pdf of the amplitude (r) is as follows:

$$pdf_r(r) = \frac{r}{\sigma^2} exp\left(-\frac{r^2}{2\sigma^2}\right). \qquad 2.18$$

And the received phase Φ distribution is uniformly distributed as:

$$pdf_\Phi(\Phi) = \frac{1}{2\pi}. \qquad 2.19$$

The mean square value of a Raleigh distributed random variable (received amplitude r) is:

$$\overline{r^2} = 2\sigma^2 \qquad\qquad 2.20$$

The product of both amplitude pdf and phase pdf gives the same distribution as the Rayleigh distribution. Thus, small scale fading without a dominant component is described as a Rayleigh distribution with the same statistical properties [13].

2.3.2.2 Small scale fading with a dominant component

Measurements and experiments done in an environment with a TX, RX and MPC, with a direct LOS (dominant component) between TX and RX, showed that the probability density function (pdf) of the received amplitude and phase, behaves the same way as the Rician distribution. A Rician distribution, shown in Figure 2.10, describes the magnitude of a complex stochastic variable whose real part is with non-zero mean value, due to LOS, Gaussian distributed, and the imaginary part is zero mean Gaussian distributed.
The pdf of the amplitude (r) is same as the Rice distribution:

$$pdf_r(r) = \frac{r}{\sigma^2} . exp\left(-\frac{r^2 + A^2}{2\sigma^2}\right) . I_0\left(\frac{rA}{\sigma^2}\right). \qquad 2.21$$

Where I_0 is the first kind Bessel function, zero order [16], A is the amplitude of the dominant component (LOS) and σ^2 is the variance.
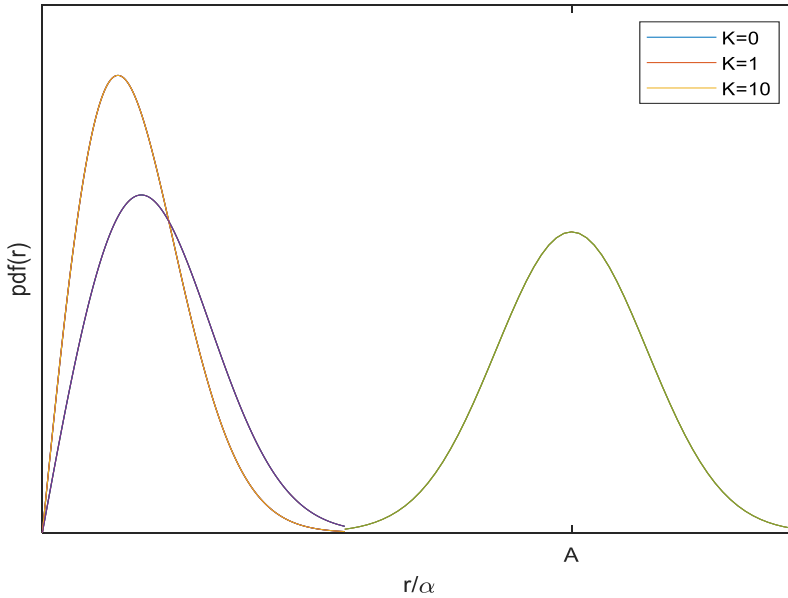
Figure 2.10: Rician distribution

The mean square value of a Rice distributed random variable (received amplitude r) is:

$$\overline{r^2} = 2\sigma^2 + A^2 \qquad 2.22$$

The rice factor K is the ratio between the line of sight (LOS) component A and the non-LOS component,

$$K = \frac{A^2}{2\sigma^2}. \qquad 2.23$$

Phase pdf is given by [17]:

$$pdf_\Phi(\Phi) \qquad 2.24$$
$$= \frac{1 + \sqrt{\pi K}.\, exp\big(kcos^2(\Phi)\big).\, cos(\Phi).\, (1 + \text{erf}\,(K.\,cos(\Phi)))}{2\pi \exp(K)}.$$

Where erf(x) is the error function calculated as [16]:

$$\text{erf}(x) = \left(\frac{2}{\pi}\right) \int_0^x exp(-t^2)\, dt. \qquad 2.25$$

As the K factor goes to zero (losing LOS component) the pdf distribution becomes similar to the Rayleigh distribution as shown in Figure 2.10.

2.3.2.3 Large scale fading

The small-scale field strength averaged over a larger spatial scale, varies due to the shadowing of the LOS and non-LOS components by other objects. Many experiments showed that the latter averaged field strength Pw plotted on a logarithmic scale gives a Gaussian distribution with mean μ. This distribution is known as log normal with pdf as:

$$pdf_P(Pw) \qquad 2.26$$
$$= \frac{20/ln(10)}{P.\sigma_P}.exp\left(-\frac{(20log_{10}(Pw) - \mu_{dB})^2}{2.\sigma_P^2}\right).$$

Where σ_P^2 is the variance and μ_{dB} is the mean value expressed in dB.

2.3.2.4 Additive white Gaussian noise

When the signal is received in the RX, it will be affected by the attenuation from the different MPC. In addition, there is the noise that effects the signal and this can be caused either by the thermal noise, which comes from the TX and RX temperature, the man-made noises, for example other electrical devices which emits over a large bandwidth, or the noisy TX and RX components (ex. Amplifiers and mixers) [13].
All of the types of noise mentioned above can be seen as uniformly distributed, since the central limit theory indicates that having many random processes summed together, gives a Gaussian (random) distribution. The

additive white Gaussian model (AWGN), has a uniform power on the frequency domain, thus the name white, which refers to the color white with the uniform emissions. AWGN is Gaussian, since the amplitudes of the noise is supposed to be normally distributed as the central limit theory indicates [13].

2.3.2.5 Doppler Spectrum

What was explained previously about the Doppler effect is applied in the simple scenario when you have one direction of movement and one signal e.g. coming from LOS. In a more complicated environment (reality), the RX will be receiving many signals from several MPC with different directions and projected speeds, hence different Doppler shifts. These variations are captured on what's called the Doppler spectrum [13].

The received power spectrum as a function of the angle between the speed direction and the signal wave, depicted as Ө in Figure 2.8, can be described as:

$$S(\theta) = \Omega[pdf_\theta(\theta)\, G(\theta) + pdf_\theta(-\theta)\, G(-\theta)]. \qquad 2.27$$

Where Ω is the mean power of the arriving wave, $G(\theta)$ is the antenna gain, $pdf_\theta(\theta)$ represents the distribution of the incident waves in terms of the arriving direction and putting into account that the waves arriving from Ө and -Ө have the same Doppler shifts.

By using Jacobean theorem, we can transform the variable Ө to f_D, which is dependent on the velocity ($|v|\, cos(\theta)$), by the following equation [13]:

$$t = \left|\frac{d\theta}{df_D}\right| = \left|\frac{1}{\frac{df_D}{d\theta}}\right| = \frac{1}{\left|\frac{v}{c}\, f\, sin(\theta)\right|} \qquad 2.28$$

$$= \frac{1}{\sqrt{v_{max}^2 - f_D{}^2}}.$$

Where c is the speed of light and $v_{max} = f_{D\,max} = fv/c$.
So, equation 2.27 becomes:

24

$$S_D(f_D)$$

$$= \begin{cases} S(\theta) . \dfrac{1}{\sqrt{v_{max}^2 - f_D{}^2}} & for - v_{max} \le f_D \le v_{max} \\ \\ 0 & otherwise \end{cases} .$$

2.29

Depending on the angular distribution and the antenna patterns different models of the Doppler spectrum can be noticed. The simplest model is known as the Jake's spectrum (bathtub). In the latter model the angular distribution is assumed to be uniformly distributed with:

$$pdf_\theta(\theta) = \frac{1}{2\pi} .$$

2.30

Hence the power spectrum becomes:

$$S_D(f_D) = \frac{\Omega\, G(\theta)}{\pi \sqrt{v_{max}^2 - f_D{}^2}} .$$

2.31

Assuming a dipole antenna with gain $G(\theta) = 1.5$ the power spectrum can be seen in Figure 2.11 taking the bathtub shape.
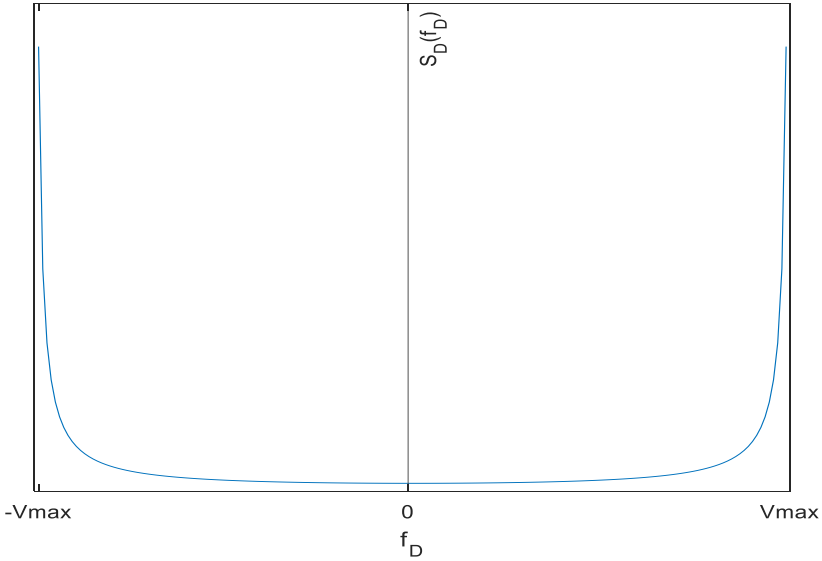
Figure 2.11: Jake's Doppler Spectrum

If the non-zero values of $S_D(f_D)$ are in the range of $f_{min} \leq f_D \leq f_{max}$ and $f_{min} = -f_{max}$ the Jake's spectrum is called symmetric Jake's as shown in the figure above. But in the other hand if $f_{min} \neq -f_{max}$ the Jake's spectrum becomes asymmetric with the power spectrum [18]:

$$S_D(f_D) = S(\theta) . \frac{A_{aj}}{\sqrt{v_{max}^2 - f_D{}^2}} \quad , \qquad\qquad 2.32$$

$$for - v_{max} \leq f_{min} \leq f_D \leq f_{max} \leq v_{max} .$$

Where:

$$A_{aj} = \frac{\pi}{\sin^{-1}\left(\dfrac{f_{max}}{f_D}\right) - \sin^{-1}\left(\dfrac{f_{min}}{f_D}\right)} . \qquad\qquad 2.33$$

The Jake's spectrum is the most commonly model used to model the Doppler spectrum. Aulin's model, which limits the non-zero values of the Jake's

Doppler spectrum and the Gaussian Doppler spectrum model are examples of alternative models [13].

2.3.3 Channel models

Channel models are used to describe the properties of the channel that have impact on the system performance. They are widely used in wireless systems' design and testing. Stochastic models and deterministic models are two types of these models.

2.3.3.1 Stochastic models

These types of models rely on the probability density function (pdf) of the channel impulse response over a large area. Hence, they don't determine the exact location's impulse response. The Rician model, which was explained in the statistical description section, is one example of such models. These types of models come in handy when designing and comparing systems.

2.3.3.2 Deterministic models

Deterministic models depend on the geographical information of the wireless communication environment and on the Maxwell's equations, this is why it's called site-specific models. These types of models need a large computational effort to get the impulse response of a certain geographic location. Deterministic models proved to be very useful in system planning and deployment [13].
Some approximations are made for the Maxwell's equations, since they require high computational effort. High frequency approximation is widely used, in which we assume that the electromagnetic waves follow the exact behavior of the geometrical optics rays [13]. Ray launching and Ray tracing are some of the methods used to model the channel deterministically.

2.3.3.2.1 Ray launching

In this method, many rays are launched from the TX into different directions. Then each ray will be followed individually. The attenuation of the Free-space, reflection or diffractions are considered for the different rays. Ray launching allows the determination of various channel characteristics [13].

2.3.3.2.2 Ray tracing

In this method, all rays travelling from the transmitter to the receiver are determined, including the reflected rays. Then, all of the attenuations are computed, hence the description of all MPC is gained.

Ray tracing becomes less efficient in wide areas, where the computational effort is increased massively since there is many reflections, scattering and diffractions occur [13].

CHAPTER 3

Methodology

In this chapter all the methods that were executed throughout this thesis is explained thoroughly, including the simulations that were carried out throughout the research.

3.1 Channel model

As was described in the theory part, channel models can be stochastic or deterministic. For designing the channel model to analyze how both the IEEE models (802.11p and 802.11bd) perform, we can pick one of the channel models to filter the signal model through.

However, our solution for designing and testing the channel model, is a bit hybrid between the deterministic approach on a simulated three dimensions (3D) environment in Unity, and stochastic approaches in the ublox-V2x simulator as can be explained in the following sections.

3.1.1 Deterministic approach

In this approach Unity 3D simulator was used to build the channel model environment in 3D. Firstly, by mapping the real environment from Google Earth to the Unity 3D simulator, we get the exact geographical locations and coordinates in 3D. The LTH area in Lund, Sweden was picked as the environment to perform simulation on. Secondly, creating two objects simulating the cars, and then making one of the cars move (transmitter TX) while the other car static representing the receiver RX in our scenario. The next step was making the roads of the map walk-able, so that the cars can move on them. Then, adding materials and colors to make the environment look as realistic as possible this can be seen in Figure 3.1.

Figure 3.1: Unity 3D's channel environment

Then the approach was to pick a portion of the environment to perform our simulation on, and then make all of the buildings in that area collides, which meant that these objects can reflect signals smoothly on their surfaces [30]. Then two signals where sent from the transmitter car's antenna (TX) and sent towards the static car's antenna (RX). One signal represented the LOS path and the other was reflected on the road using Snell's law of reflection. Note that in our scenario we assume omnidirectional antennas, signals are radiated in all directions with equal energy. We also assume that this environment is in free space and as long as we have a LOS path, we have road reflection as can be seen in Figure 3.2. The TX will first store the objects, representing the buildings within a certain radius from its location and then calculates the reflection points on them using the RX's exact 3D position. Then those rays will be traced to check if they reach the RX without getting blocked after the reflection. The 3D reflection point calculations were done with the same idea of section 2.3.1.3.1.
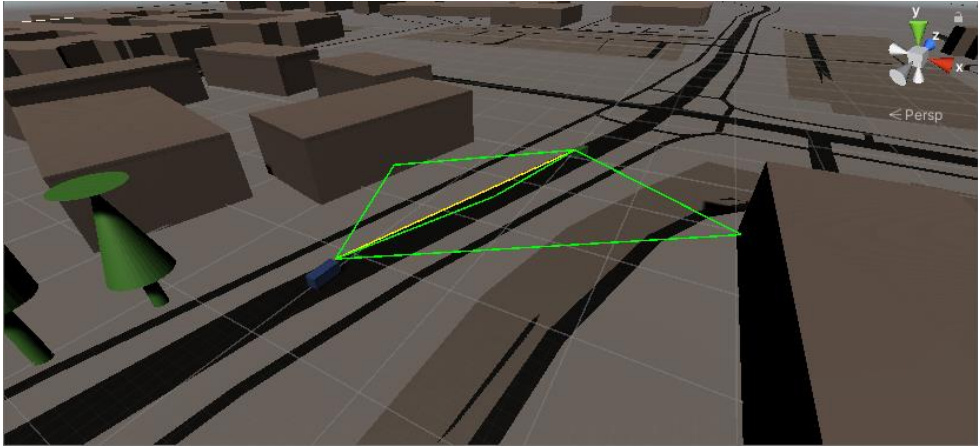
Figure 3.2: LOS and non-LOS components

Lastly, incidence angles, diffraction angles if a diffraction occur, Doppler shifts angle and the distances of both LOS paths and non-LOS paths are stored in a comma separated values (CSV) file. The storing step is for getting the channel impulse response calculated, hence the channel model of this exact 3D scenario (deterministic model). The latter simulation is done in MATLAB, using the power received calculations described in the theory chapter.

3.1.1.1 Reflection point calculations

The TX will store the objects within the 3D radius and extract the vertices of those objects. From the 3D vertices of the building we can find the surfaces (walls) that can reflect the signal towards the RX and exclude the other surfaces. The latter is done by ray tracing and checking if the ray can reach RX location. To determine a wall surface, the normal 3D vector of the vertices is checked, since same normal vectors show that vertices belong to the same wall. As can be seen in Figure 3.3, vertices x6, x1, x2 and x3 have the same normal vector, this is the result of them being on the same wall (surface).
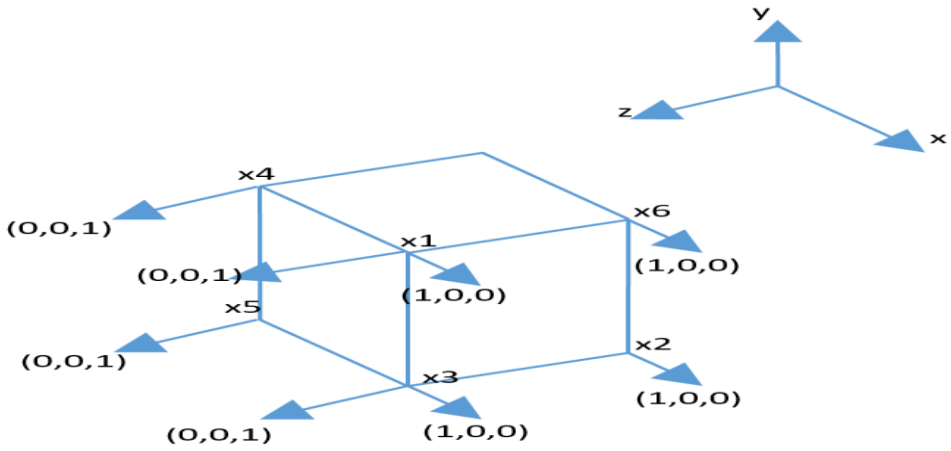
Figure 3.3: Building Vertices

The next step is applying the equations from [3.1 - 3.7] to get the exact 3D position (P) where the reflection happens. Then check if this point is within the wall vertices, between v_1 and v_2 in the figure below.
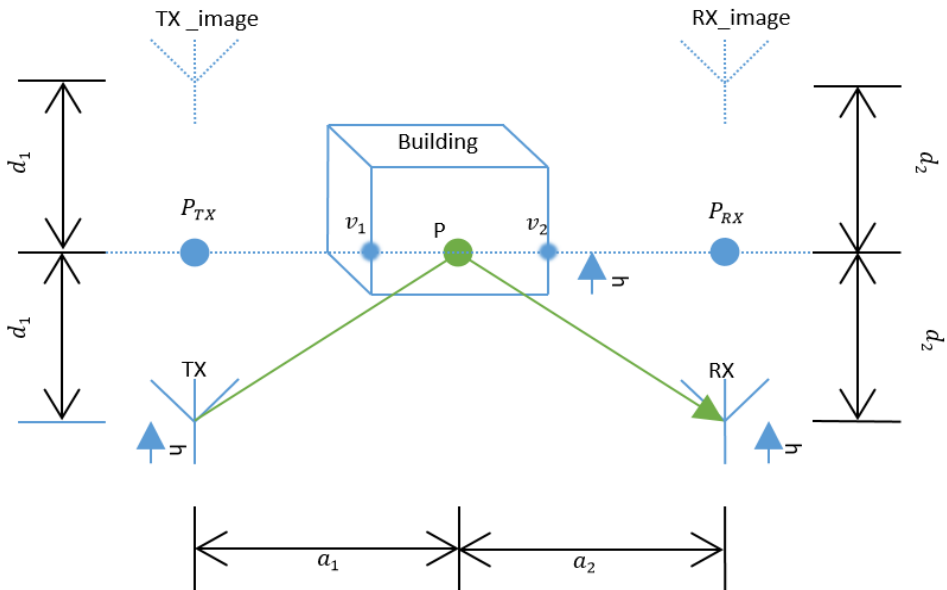

Figure 3.4: Reflection point

From the simulator we have h as the antennas' height, TX and RX positions in 3D, and vertices of the building. Using equation 3.1, we can find the reflection point P as section 2.3.1.3.1 described.

$$P = P_{RX} + n \cdot a_2 .$$
3.1

Where $n = \frac{P_{RX} - P_{TX}}{\|P_{RX} - P_{TX}\|}$, P_{RX} and P_{TX} represent projections of RX and TX respectively to the wall's plane and can be found using Figure 3.5 and by getting the vector between v_2 and RX location (RX_L).

$$\vec{r} = v_2 - RX_L .$$
3.2

We define Θ as the angle between the normal vector of $\overrightarrow{v_2}$ and $\vec{r}$. And to obtain d_2, which is the distance between the 3D points v_2 and RX_L , we just perform this equation:

$$d_2 = |\vec{r}| . \cos(\Theta).$$
3.3

Then RX image location will become:

$$RX_{image_L} = RX_L - 2 \, d_2 . \overrightarrow{v_2} .$$
3.4

Since the vector between the RX and its image is the product of the distance between these two points ($2 \, d_2$) and the unit vector $\overrightarrow{v_2}$.

Moreover, P_{RX} can be calculated as the middle point between the RX image position and the actual RX position:

$$P_{RX} = \frac{RX_L + RX_{image_L}}{2} .$$
3.5

In the same manner P_{TX} becomes:

$$P_{TX} = \frac{TX_L + TX_{image_L}}{2} .$$
3.6
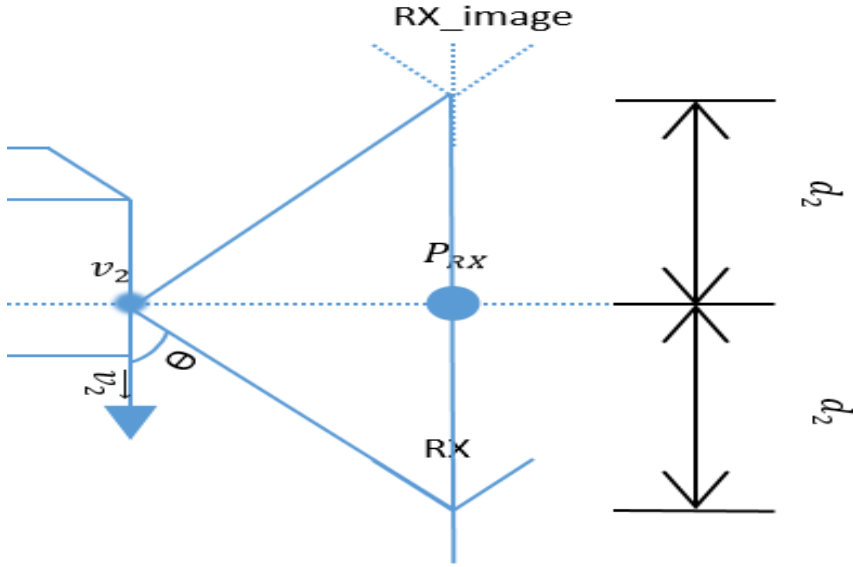
Figure 3.5

After finding P_{RX} and P_{TX} points on Figure 3.4, P in 3D can be calculated as the following:

$$P = P_{RX} + \frac{P_{RX} - P_{TX}}{\|P_{RX} - P_{TX}\|} \cdot a_1 \qquad\qquad 3.7$$

$$= P_{RX} + \frac{P_{RX} - P_{TX}}{1 + d_2/d_1}.$$

Since, $a_1 = \frac{\|P_{RX} - P_{TX}\|}{1 + d_2/d_1}$ by solving equation 2.8 and 2.10. Where h_r and h_t represents d_2 and d_1 respectively in this case.

3.1.2 Stochastic approach

In [19], the channel model taken from the real environment is estimated by using the stochastic approach and then the IEEE signal models were tested on this model using ublox-V2x simulator. For our scenario, we know that we get from the Unity 3D simulator the channel data every time instant, which means that between these time instants we have no channel data stored. Hence, stochastic approach comes in handy, where we compensate for the delays between every deterministic channel data we get from Unity 3D and estimate the channel model from the time instant until the next time instant occurs. The latter is done using the Rician model, since we know in our scenario that there will always be a LOS path. On the other hand, the Doppler spectrum, asymmetric Jake's spectrum model is used as was explained in the theory part. Combining stochastic and deterministic methods increases the efficiency and accuracy of the model [13].

3.2   Channel impulse response

The calculations done to get the channel impulse response was executed in MATLAB. Two methods were used to find the channel impulse response:

3.2.1   Hybrid method

This is where the deterministic channel data is mixed with the Rician model (stochastic) simulation in MATLAB, to enhance the design of the channel model.

3.2.1.1 Deterministic channel calculations

Equations 2.15 and 2.16, show how to get the LOS channel component R_{LOS} and the non-LOS component $R_{non-LOS}$. From these components we can get a description of the channel h_i at every time instant (i) we get the data from Unity 3D, in which includes the LOS path and other non-LOS paths:

$$h_i = \left[R_{LOS_0}, R_{non-LOS_1}, R_{non-LOS_2}, R_{non-LOS_3} \dots R_{non-LOS_N} \right]. \qquad 3.8$$

Then by using Rician, Rayleigh channel models and an Asymmetric Jake's Doppler spectrum model in MATLAB, we can get a better description of the channel and compensate for the lack of data between every time instant. The latter models need to get the Doppler shift, and the delays of each path as shown below:

$$\tau_i = \left[\tau_{LOS_0}, \tau_{non-LOS_1}, \tau_{non-LOS_2}, \tau_{non-LOS_3} \cdots \tau_{non-LOS_N}\right],$$

$$and \; f_{D_i}$$
$$= \left[f_{D_{LOS_0}}, \; f_{D_{non-LOS_1}}, \; f_{D_{tnon-LOS_2}}, \; f_{D_{tnon-LOS_3}} \cdots \; f_{D_{non-LOS_N}} \right].$$

3.9

Where τ is the delay and is calculated as the total propagation distance divided by the speed of light, f_{D_t} is the Doppler shift and can be calculated for the LOS as in equation 2.13 where N is the number of the fading paths (non-LOS paths) every time instant. For the non-LOS Doppler shift calculations, same equations used for LOS are valid but the velocity is calculated towards the direction of the reflection point (or RX_image as seen in Figure 3.4), not towards the RX direction as in the LOS situation.

3.2.1.2 Rician and Rayleigh channel model Simulation

As [20] describes how to simulate the Rayleigh and Rician channel models in MATLAB by the use of band-limited discrete multipath propagation models, in which it is assumed that the power delay profile and Doppler spectrum are separable (Wide Sense Stationary Uncorrelated Scatterers WSSUS) [20]. The output of the channel y_t in relation with the input samples x_t to the channel can be found by:

$$y_i = \sum_{n=-N_2}^{N_1} x_{t-n} \cdot g_n.$$

3.10

Where g_n are the tap weights which can be found with:

$$g_n = \sum_{i=0}^{N} \alpha_i . sinc\left(\frac{\tau_i}{T_s} - n\right) . \qquad \text{3.11}$$

The input sampling time is T_s, while N_1 and N_2 are picked so that the magnitude of the tap weight is small outside the bound $(-N_2, N_1)$. The uncorrelated complex path gains α_i can be found from the equation below [20]:

$$\alpha_i = \sqrt{\Omega_i} . \left[\frac{z_i}{\sqrt{K_i+1}} + \sqrt{\frac{K_i}{K_i+1}} . e^{2\pi f_{DLOS_0}t+\theta}\right] . \qquad \text{3.12}$$

Where K_i is the Rician factor of the i'th path, θ is the phase of the line of sight (LOS) path and z_i contains the in-phase μ_{in} and quadrature μ_Q components through the following equation [20]:

$$z_i(t) = \mu_{in_i}(t) + j . \mu_{Q_i}(t). \qquad \text{3.13}$$

Where Ω_i is the mean value of the h_i values.
The in-phase and quadrature components are found by using the sum of sinusoids technique, which is described in [21,

$$\mu_i(t) = \sqrt{\frac{2}{S_i}} \sum_{n=1}^{S_i} \cos(2\pi f_{D_{i,n}}t + \theta_{i,n}) . \qquad \text{3.14}$$

Where S_i is the number of sinusoids used to model a single path, t is the fading time, and $\theta_{i,n}$ is the phase of the n-th component of a certain path. For a Jake's Doppler spectrum model, the Doppler frequency component in equation 3.9 with a maximum shift of $f_{D_{max}}$ is calculated as:

$$f_{D_{i,n}} = f_{D_{max}} \cos\left(\frac{\pi}{2S_i}\left(n - \frac{1}{2}\right) + \alpha_{i,0}\right) . \qquad \text{3.15}$$

Where:

$$\alpha_{i,0} \triangleq \begin{cases} \dfrac{\pi}{4S_i} \cdot \dfrac{i}{N+2} & , if \ \mu = \mu_{in} \\ -\dfrac{\pi}{4S_i} \cdot \dfrac{i}{N+2} & , if \ \mu = \mu_Q \end{cases} . \qquad 3.16$$

Therefore, in MATLAB to simulate the channel these inputs are the most required:

1. The LOS or non-LOS components of each path (h_i), most of the times these values are normalized in a way that the total average power over time is 0dB.
2. The separate path delays (τ_i), the first delay path (the LOS in our scenario) is always considered as zero.
3. The input sampling rate ($1/T_s$).
4. The Rician factor of each path (K_i), when it's a zero value it represents that this path is Rayleigh fading.
5. The LOS initial phase (Θ).
6. The Doppler shift of the LOS path ($f_{D_{LOS_0}}$).
7. The maximum Doppler shift of all paths ($f_{D_{max}}$).
8. The Doppler spectrum for each path.

Note that the Doppler spectrum of each path can be structured as an Asymmetric Jake's spectrum as described in the theory part and by using equations 2.32 and 2.33, in which f_{min} and f_{max} can be seen as the minimum and maximum Doppler shifts of the given paths respectively [22].

In our scenario by getting the channel model every time instant with the same statistical description as the Rician or Rayleigh distribution, depending on the path, we combine our deterministic channel data with the stochastic Rician model. Thus, we have a better description of the total channel impulse response. Note that in the Rician model when K is zero that means the corresponding path is Rayleigh distributed.

3.2.2 Direct method

Since we know that we get our data from Unity 3D with delays between every time instance, the best description for the channel impulse response can be done by using the tapped delay line model for wide band signals [13].

By using the tapped delay model, the channel impulse response $h(t,\tau)$ becomes:

$$h(t,\tau) = a_0\delta(\tau - \tau_0) + \sum_{i=1}^{N} c_i(t)\delta(\tau - \tau_i) \qquad 3.17$$

Where a_0 is the LOS component and $c_i(t)$ is the complex zero mean Gaussian process associated with Doppler spectrum.

The best description for the channel impulse response can be done by using the tapped delay line model for wide band signals [13]. The most commonly used N-tap wide band model is Rayleigh fading model.
To exhibit delay dispersion, a stochastic fading channel is used with a limited number of taps (i.e. N=2) and LOS components are removed. Hence it is known as a two-paths channel or two-delays channel [13]. For LOS connection the number of taps is reduced (i.e. N=2) and delay τ_0 is not constant as τ_1, it differs. Hence instead of stochastic, this channel is a rician channel with flat fading for $\tau_0 = \tau_1$ [13].

3.2.2.1 Sinc function

A sinc function is an even function with Unity 3D area, where the pulse flows through all positive and negative integers [4]. To avoid Inter-symbol interference, the sinc plot reaches a maximum value of 1 at time interval 0 (i.e. t = 0). The result of a sinc function and some other signal would likewise ensure zero intersections at all positive and negative integer values [4]. Sinc function is basically defined by:

$$g(t) = \frac{\sin(\pi t)}{\pi t} \overset{\Delta}{=} \text{sinc(t)} \qquad 3.18$$

3.2.2.2 Channel Matrices

Time-variant, double-directional and complex channel frequency transfer functions of different multipath components should be modeled using channel matrices [14]. These MPCs are modeled using the transfer function is explained in the below equation. These channel matrices are basically formed for different propagation paths from the LOS, road/ground reflection, and reflections from the other reflecting objects. When the vehicle moves from initial the position to the destination, the radio channel between TX and RX may consist of a different MPC, so at each MPC the distance from initial position to reflection point and to the destination it has certain distances. By using transfer function, it is possible to store "n" number of MPC in a channel matrix.

$$H(k) = \left(\left(\frac{\lambda}{4\pi d}\right) * a_{LOS}\right) * \left(e^{j2\pi(fk+fd\_LOS)*\frac{d}{c}}\right) + \left(\left(\frac{\lambda}{4\pi d_1}\right) * a_{road}\right) * \left(e^{j2\pi(fk+fd\_road)*\frac{d_1}{c}}\right) +$$

$$\left(\left(\frac{\lambda}{4\pi d_3}\right) * a_{NLOS1}\right) * \left(e^{j2\pi(fk+fd\_NLOS1)*\frac{d_1}{c}}\right) + \ldots\ldots\ldots$$

Figure 3.6: Transfer function

Where λ_k is the wavelength of the k-th subcarrier, c is the speed of light (3x10^8 m/s), a_{LOS} is the amplitude of Line of sight (LOS), fd_LOS is the Doppler shift of LOS, fk is the sub carriers frequency, a_{road} is amplitude of road or ground reflection depending on the material, fd_road is the Doppler shift road reflection, a_{NLOS1} is the amplitude of the first non-LOS path, d1, d2, d3 are the distances of LOS, road and non-LOS paths. The channel response/transfer function in the time domain is obtained by taking Inverse Fast Fourier transform (IFFT) of the transfer function in the frequency domain.

3.3 Ublox-V2x simulator model

Ublox-V2x simulator is an open source simulation model, which was suggested by ublox. It is useful in V2x communications research [23]. The main idea of this simulator is to create different stochastic channel models and measure the performance of V2x signal models, using IEEE 802.11p or 802.11bd (described in the theory part), in these channel models. The channel model creation is using the idea from, Rician and Rayleigh channel model simulation section. These signal models can be tested for different modulation and coding schemes. After convolving the signal model with the channel model, the simulator obtains the received signal and then after adding AWGN and phase noise, the final received signal is created. The next step of the simulator is to find the synchronization point of the signal from the preamble pilot, then do channel estimation, get the received packets and check the errors and the throughput.

The performance of these signal models is measured by the Packet Error Rate (PER) and throughput for different Signal to Noise Ratio (SNR) values and is done for several iterations to get a better result. The iteration technique used is the Monte-Carlo iterations.

Simulation performance can be enhanced by the use of compiled MEX files for the high-level transmitter and receiver functions. The MEX files help to accelerate the MATLAB simulation [23].

3.3.1 Ublox-V2x simulator with hybrid channel model

In our scenario, by using the simulator we combine the stochastic model of the simulator and our deterministic channel data to get an enhanced channel model description. The next step is calculating the exact average SNR value of every time instant for a fixed noise floor of -100dBm. Where dBm is the decibel scale when compared to 1milliwatts. Then the same signal models of the simulator are used to be convoluted with our hybrid channel object. After that, the calculated values of SNRs are used in the stage where AWGN and phase noise are added (as seen in the previous section). After the channel estimation and the determination of errors, the PER and throughput is calculated for every time instant. This calculation is repeated for every time instant (channel model) for multiple Monte-Carlo iterations to get the communication performance statistics.

3.3.2 Performance measurement

The performance of the IEEE signal models is measured in terms of packet error rate and throughput.

3.3.2.1 Average Packet error rate

Received packets are determined to be erroneous if one of the following occurs:

- Packet is not detected. The latter is determined after estimating the synchronization point of the signal, from the preamble pilot. If the synchronization point is not valid the packet is assumed to be not detected.
- Signal error, which can happen if the even parity check of the first part of the received bits, after channel calibration and decoding, is not valid. In addition, signal error can happen if the decoded length of signal is not a valid number or the coding and modulation scheme determined from the first four bits is not valid. Lastly, if the payload length or the number of OFDM symbols is not the same as the stored values, signal is not received correctly.
- Data error, this is determined from a Cyclic Redundancy Check CRC32 check done to the payload bytes. If the CRC check founds errors, the data is assumed to be with errors and the whole packet is lost.

If any of the errors above happens, we assume we have a one packet error rate (PER). If none of the errors occur, the simulator assumes zero PER. By calculating the PER for different iterations (N) we can have the average PER as a better performance measurement parameter,

$$avgPER = \frac{\sum_{i=1}^{N} PER(i)}{N}. \qquad 3.19$$

3.3.2.2 Throughput

To calculate the throughput, the simulator assigns an efficiency factor (eff) if the signal model is IEEE 802.11p this factor will be with value 1. On the

other hand, for the IEEE 802.11bd signal model this value is dependent on the mid-amble period (mid) where eff will be:

$$eff = \frac{mid}{mid + 1}.$$ 3.20

And then the average throughput in Megabits per seconds (Mbps) can be found from:

$$\text{avg throughput} = (1 - \text{avgPER}) * D.$$ 3.21

Where:

$$D = \frac{eff.N_{dsc}.dbps.bpscs}{8.cbps}.$$ 3.22

And N_{dsc} is number of data subcarriers, bpscs is the number of bits per modulation symbol, cbps and dbps are the number of the coded and decoded bits per Subcarrier respectively.

CHAPTER **4**

Results

In this chapter all of the results from the simulations performed in Unity 3D game engine and MATLAB are presented.

4.1 Channel model results

After simulating the 3D channel environment in Unity 3D with a scenario as shown in Figure 4.1, the channel data is collected. Figure 4.2 depict the received power at the receiver side for a 1watts transmitted power and neglected noise.
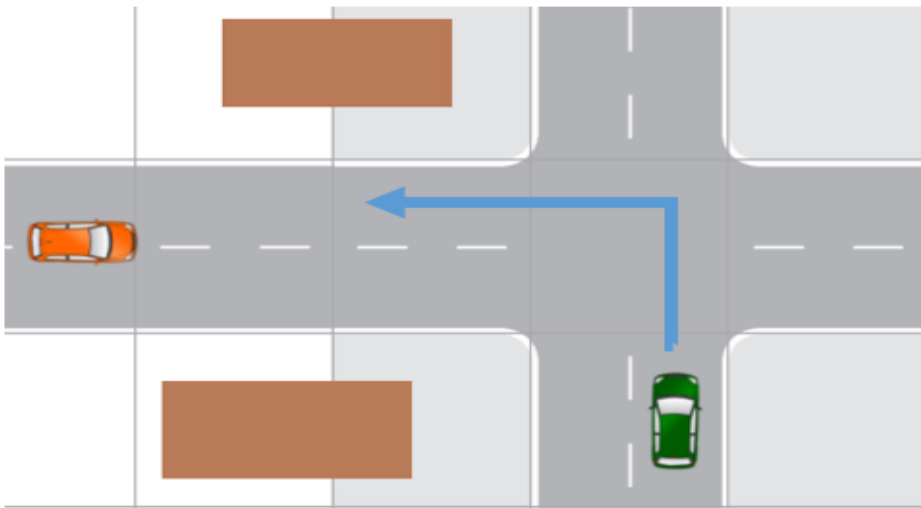
Figure 4.1: Unity 3D's Urban LOS scenario

In the scenario depicted in the previous graph we always have LOS component and non-LOS component coming from the road reflection. There are also two other non-LOS components coming from the buildings whenever there is a reflection.

The assumptions and parameters which were chosen to create this environment are:

- Minimum number of components arriving at the receiver (RX) side per time instant is two components. Representing the LOS component and non-LOS component reflected from the road.
- Maximum number of components at RX per time instant is four components.
- The environment is simulated in free space.
- Antennas are isotropic with gain of 0dB.
- Single antenna at TX and single antenna at Rx (SISO).
- 30 dBm of transmitted power.
- Smooth surfaces on the road and the buildings, thus Snell's law of reflection is valid for all reflections.
- Ground is made of Asphalt with permittivity of 3.5 [24].
- Buildings made of concrete with permittivity of 5 [25].
- The car which have the transmitter antenna is moving while the other car is static.
- Car speed is 3.5 m/s (12.6 km/h).
- Carrier frequency of 5.9 GHz.
- Neglecting the noise component. As it will be added later in ublox-V2x simulator.
- Wide sense stationary and uncorrelated scatterer assumptions. In which different Doppler and different delay contributions are uncorrelated [13].
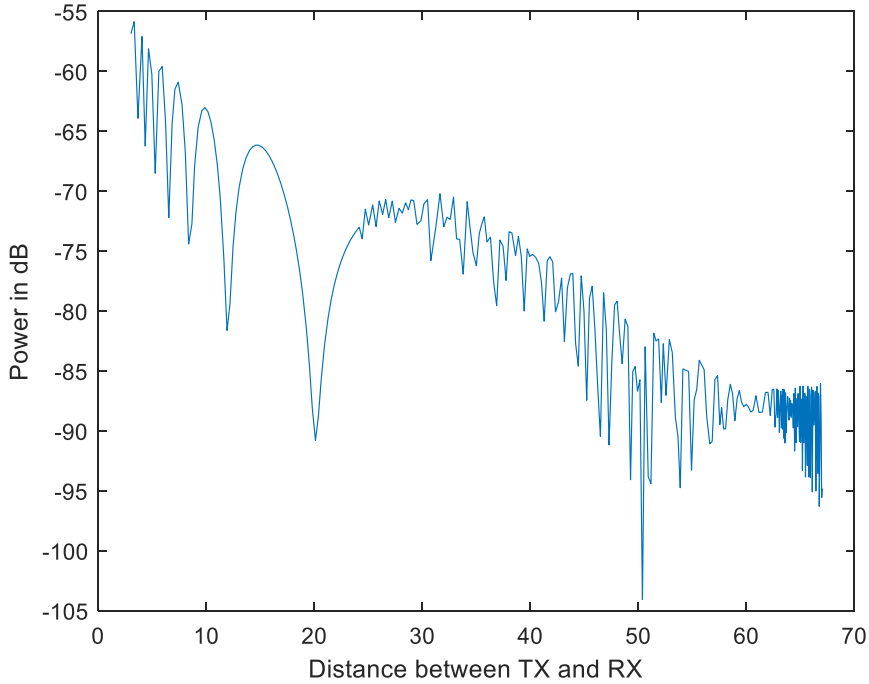
Figure 4.2: Received power

As can be seen in the figure above, due to the reflections of the buildings, the road and the LOS path we have these fluctuations as discussed in the theory chapter (Chapter 2). The fluctuation between the 26-67 meters is caused by the reflection from the buildings. As we get closer to the Receiver car (orange car in Figure 4.1) the LOS becomes more dominant and the fluctuation occurs only from the road reflection.

4.1.1   Deterministic linear time variant channel

The channel can be described using the tapped delay model. After applying the formula in equation 3.17 we can get a description of the discrete channel impulse response $h(t, \tau)$, also called as the finite impulse response (FIR), varying with time and delay as shown in Figure 4.3.
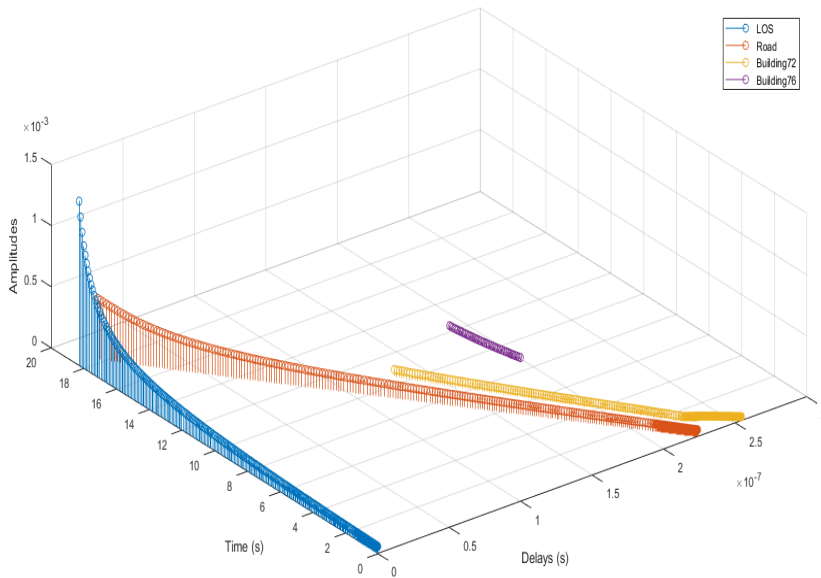
Figure 4.3: Discrete channel impulse response

It can be seen that when the transmitter car comes closer to the static car, the $h(t, \tau)$ becomes stronger and the attenuation is weaker. Since the attenuation is proportion to distance as discussed in Chapter 2.

The Doppler frequency shifts are of positive values that is a result of the movement of TX being towards RX.

4.1.2 Sinc function

The normalized sinc plot Figure 4.4 is obtained by considering the theoretical values (Channel Bandwidth (10MHz) and the signal's sampling frequency) of IEEE 802.11p and thus Equation 3.8 is formed after considering exact sampling time to plot the signal [4]. This plot is formed for the smoothness of the channel model signal.

47
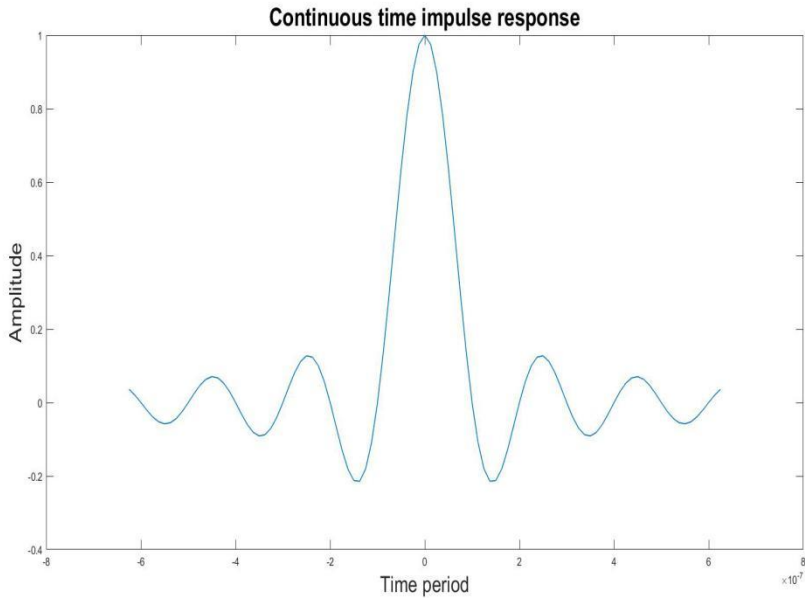
Figure 4.4: Sinc signal

4.1.3   Channel impulse response from the transfer function

The equation 3.8 is used to plot the discrete time impulse response of the signal. Figure 4.5 depicts the discrete channel impulse response of a single time instant.
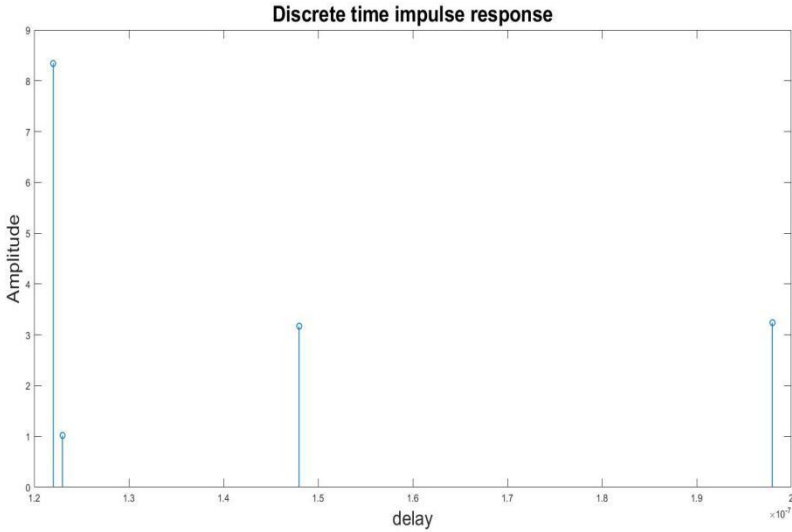
Figure 4.5: One instant discrete impulse response

We can obtain the transfer function of LOS, road, and buildings. By considering fft size (k =64 for 802.11p) in MATLAB, frequency impulse response of channel is plotted for each time instant (distance) by considering absolute values, as the vehicle moves from the initial position to the destination, we get certain delays and amplitudes. Figure 4.6 is created using the equation on figure 3.6.
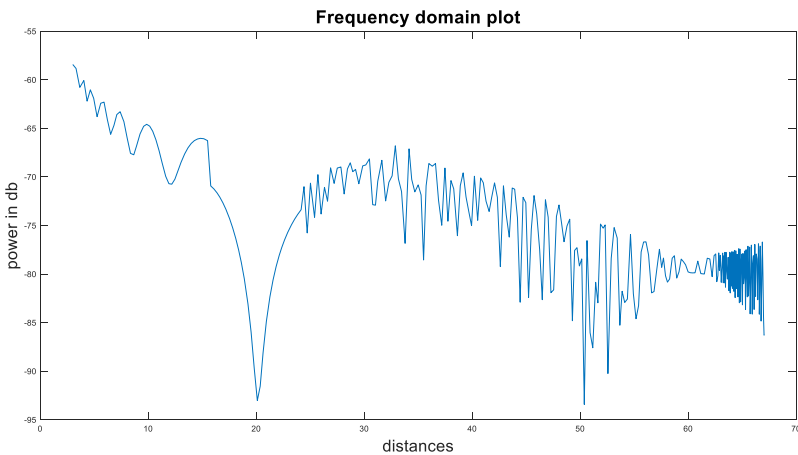
Figure 4.6: $\sum_{k=0}^{N_{fft}} |H(f_k)|$ vs LOS Distance

4.2 V2x simulator model

In this section, the results of both the average throughput and packet error rate are shown for both of the stochastic channel models that were taken from the measurements done in reality [26] and the channel data that was taken from the Unity 3D game engine.

4.2.1 Stochastic channel obtained from real measurements

The figures from Figure 4.7 to Figure 4.18 shows the performance of a pure AWGN channel, Rural LOS area measurements, Urban LOS area measurements and a street crossing non-LOS measurements with using the channel model values described in Table 4.1, Table 4.2 and Table 4.3 by using SNR values ranging from 0-25 dB [19]. For more details regarding the measurements and the V2x simulation model you can check [19] and [26].

	Tap1	Tap2	Tap3
Power	0dB	-14dB	-17dB
Delay	0ns	83ns	183ns
Doppler	0Hz	492Hz	-295Hz

Table 4.1: Rural LOS parameters

	Tap1	Tap2	Tap3	Tap4
Power	0dB	-8dB	-10dB	-15dB
Delay	0ns	117ns	183ns	333ns
Doppler	0Hz	236Hz	-157Hz	492Hz

Table 4.2: Urban approaching LOS parameters

	Tap1	Tap2	Tap3	Tap4
Power	0dB	-3dB	-5dB	-10dB
Delay	0ns	267ns	400ns	533ns
Doppler	0Hz	295Hz	-98Hz	591Hz

Table 4.3: Crossing non-LOS parameters

50

The MCS (modulation and coding schemes) values are explained in Table 4.4.

| MCS value	Coding rate	Modulation type
0	1/2	BPSK
1	3/4	BPSK
2	1/2	QPSK
3	3/4	QPSK
4	1/2	16-QAM
5	3/4	16-QAM
6	2/3	64-QAM
7	3/4	64-QAM

Table 4.4: MCS
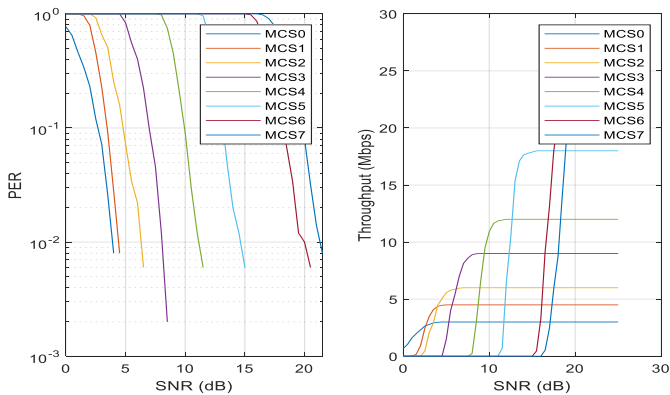
Figure 4.7: Performance of 802.11p signal model on AWGN channel
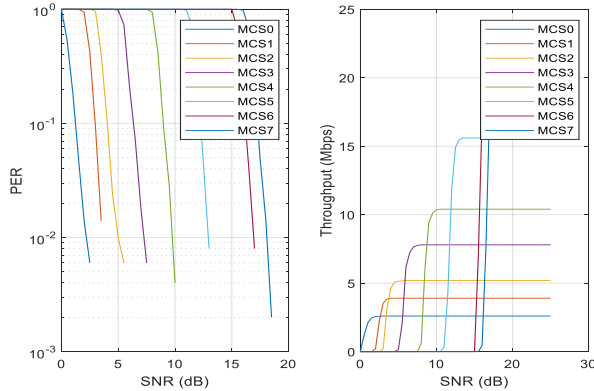
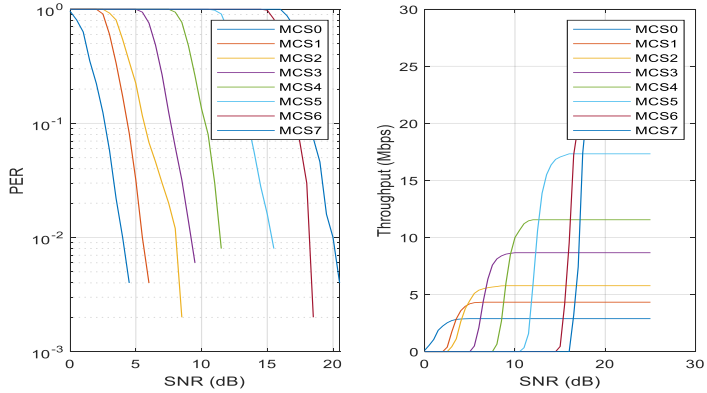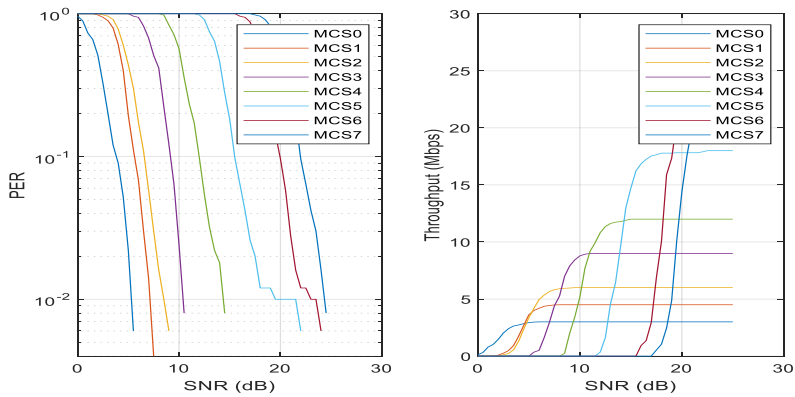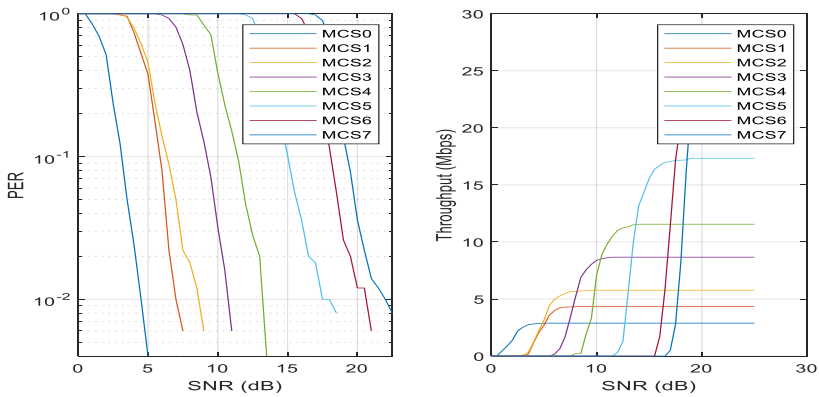Figure 4.8: Performance of 802.11bd signal model (4 mid-amble period) on AWGN channel
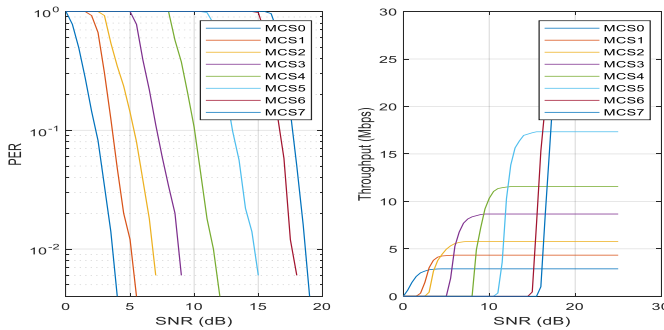
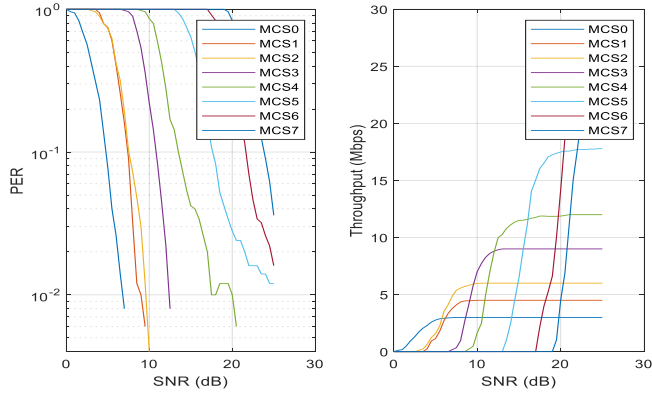Figure 4.9: Performance of 802.11bd signal model (8 mid-amble period) on AWGN channel

From the AWGN performance figures above, it can be seen that for the 802.11p signal model we can get higher throughput. However, we need a higher SNR value to maintain a reasonable PER. Using 802.11bd signal model gives a better PER, while a lower throughput for each MCS value is noticed. The lower throughput is caused by adding the mid-amble pilots, which decreases the spectral efficiency [11].

The Rural LOS measurement is done where there is no other MPC; only two cars, one of which is moving with a high speed of 144km/h. In the urban scenario, the cars are moving towards each other (an average speed is around 119km/h) in a dense urban environment. Lastly, the crossing scenario includes two cars moving in an intersection in an urban environment with

blocked LOS in the beginning of the movement and with a maximum speed of 126km/h [19].
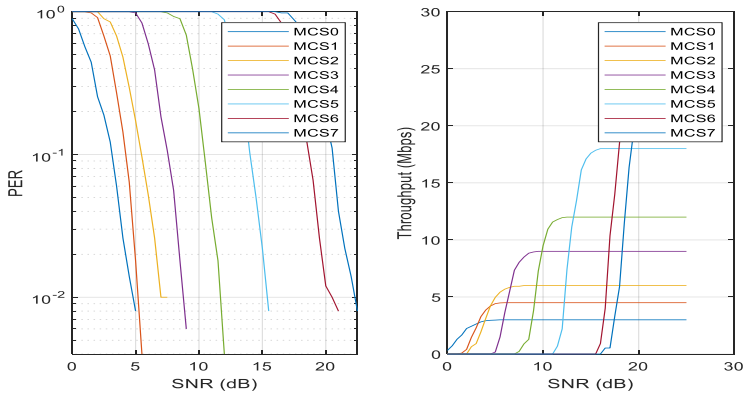
Figure 4.10: Performance of 802.11p signal model on rural LOS channel
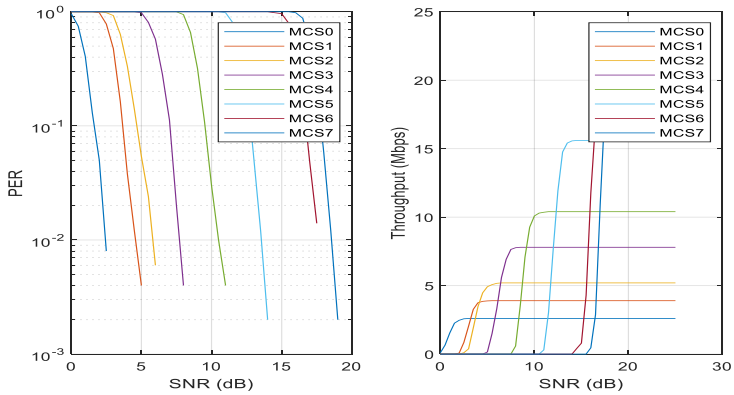
Figure 4.11: Performance of 802.11bd signal model (4 mid-amble period) on rural LOS channel

Figure 4.12: Performance of 802.11bd signal model (8 mid-amble period)
on rural LOS channel

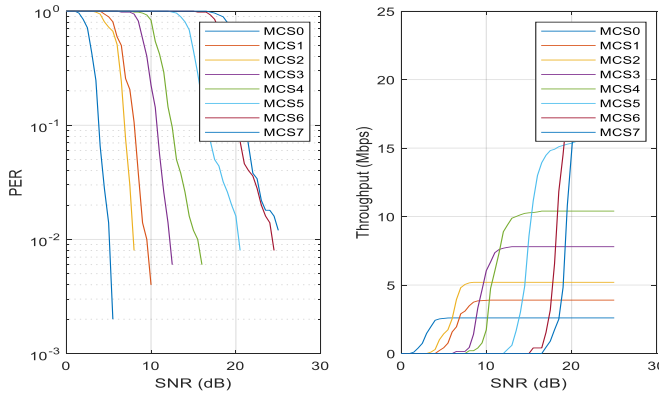Figure 4.13: Performance of 802.11p signal model on Urban LOS channel
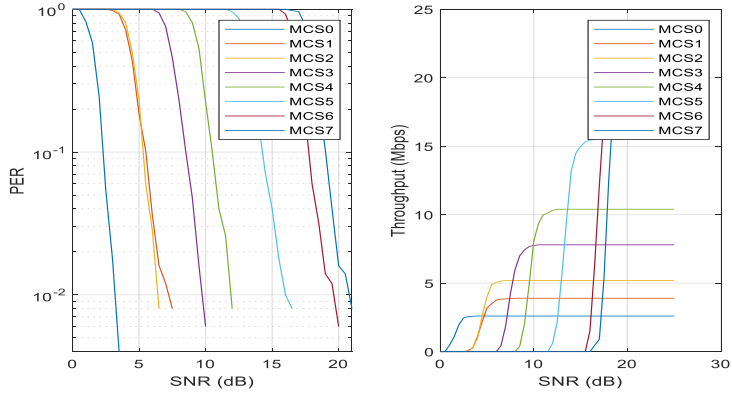
Figure 4.14: Performance of 802.11bd signal model (4 mid-amble period) on Urban LOS channel

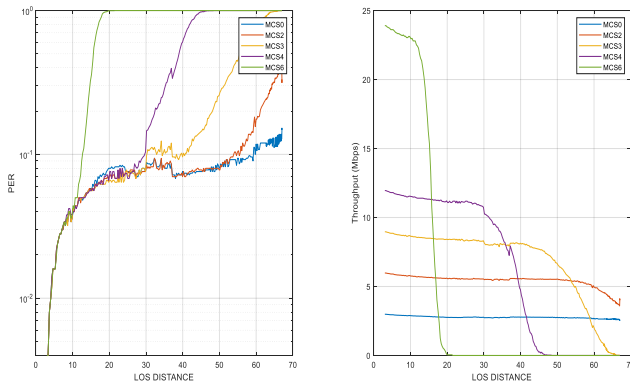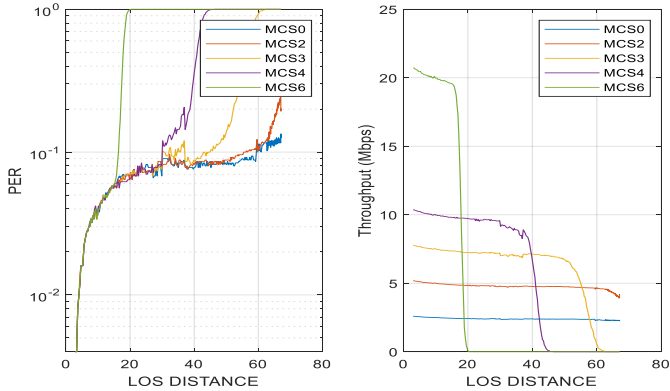Figure 4.15: Performance of 802.11bd signal model (8 mid-amble period) on Urban LOS channel

Figure 4.16: Performance of 802.11p signal model on the crossing channel

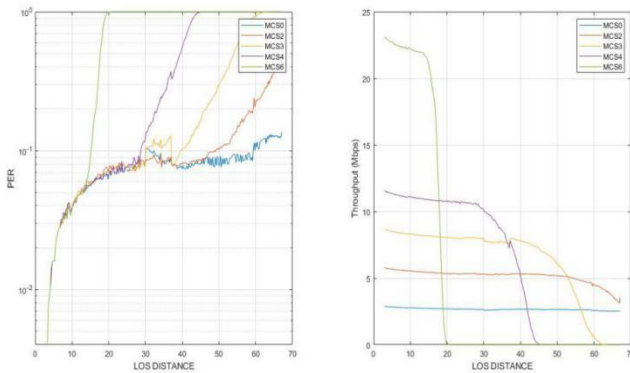Figure 4.17: Performance of 802.11bd signal model (4 mid-amble period)
on the crossing channel

For the different scenarios it can be seen that the performance of the rural
LOS and the urban LOS scenarios are quite similar. Since these scenarios
have a dominant LOS, they are used as a reference for other measurements.
It can be seen that the street crossing scenario is different since there is no
LOS component and the performance of the IEEE signal models is dependent
on the non-LOS propagation path. Hence, more energy should be consumed
in terms of SNR to get a similar performance to the LOS scenarios.
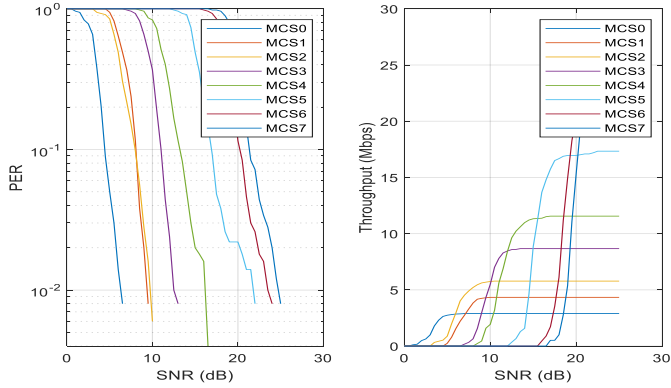
Figure 4.18: Performance of 802.11bd signal model (8 mid-amble period) on the crossing channel

4.2.2 Ublox-V2x simulator using the hybrid channel model approach

By taking the data, we got from the Unity 3D deterministic channel model, we feed it at every time instant to the V2x simulator model we get a description of the performance for MCS (0, 2, 3, 4 and 6) from the time the car starts moving until it reaches the destination (the static car), as seen in Figure 4.19, Figure 4.20 and Figure 4.21. Since this is a LOS scenario, it was expected to get a similar performance to the urban LOS scenario.

Figure 4.19: Performance of 802.11p signal model on the 3D Unity 3D channel

Figure 4.20: Performance of 802.11bd signal model (4 mid-amble period)
on the 3D Unity 3D channel

Figure 4.21: Performance of 802.11bd signal model (8 mid-amble period)
on the 3D Unity 3D channel

It can be seen from the figures above (4.7-4.22) that the performance in terms
of PER drops when using a higher coding and modulation scheme. Since the
dependency is on the SNR values, and for higher MCS we need a higher SNR
to maintain the same performance. In our scenario the value of the SNR
depends on the distance between the TX and RX and the non-LOS
components. It can be seen in Figure 4.19, Figure 4.20 and Figure 4.21, that
when LOS component becomes dominant (small distance between TX and
RX) the SNR value becomes stronger, hence a better average PER and
throughput is obtained.

In the other hand, the same performance enhancement that is seen on the previous section is also valid here When moving from 802.11p signal model to 802.11bd, we can have a slightly better PER performance and a lower throughput. The latter is the result of using the pilots. Moreover, we can acquire a better throughput by using the eight mid-amble period pilots in the expense of a slightly higher PER.

CHAPTER **5**

Conclusions and future work

5.1 Conclusions

V2x that is based on WLAN uses either IEEE 802.11p or IEEE 802.11bd signal models. To get a better understanding on the performance of both signal models, V2x simulation model is used. In this model the IEEE 802.11bd does not have the complete set of features. However, the most important features are included such as LDPC channel coding and the mid-ambles pilots. V2x simulation model builds the channel model according to the data from the real time measurements, considered within several taps of delays. Our proposed alternative way, by getting the channel information from a 3D simulator, gave the results of the performance of the IEEE signal models as seen in Chapter 4.

After analyzing these signal models with the various stochastic channels and our hybrid approach, it was observed that the performance of these signal models is a trade-off between the throughput and PER. The results from the deterministic channel model (taken from Unity 3D) gave the expected performance depending on the distance between the transmitter and receiver, since the LOS is the most dominant component in the 3D scenario. For a fixed level of noise, the SNR will be highly affected by the path loss.

High modulation schemes need high SNR values, as can be seen in the Urban LOS performance figures. On the other hand, the Unity 3D channel performance figures show that when the distance is near (SNR high) we get a better performance from that modulation scheme. From the latter, we can say that Urban LOS scenario performance was almost similar to our Unity 3D channel simulation.

5.2 Future work

Several aspects can be considered as future work:

- Simulating different scenarios for the deterministic channel model, with relaxing the assumptions made, to get a more realistic channel models such as simulating highway scenarios, covering wider ranges of distances, and adding more non-LOS components.
- Finding new features and enhancements on the IEEE 802.11bd signal model. Since ublox-V2x simulator model did not use the complete features of 802.11bd e.g. considering MIMO.
- Analyze and simulate V2x for the 3GPP signal models (using LTE and 5G). In our research we only focused on the IEEE (WLAN) signal models.

References

[1] Pin-Han Ho, Hong Wen, Guang Gong, "A Novel Framework for Message Authentication in Vehicular Communication Networks", Department of Electrical Computer Engineering, University of Waterloo, Canada, published by IEEE on 04 March 2010.

[2] L.Nassar, A.Jundi, K.Golestan, Farook Sattar, Fakhri Karray, Mohammed S. Kamel, Slim Boumaiza, "Vehicular Ad-hoc Networks(VANETs): Capabilities, Challenges in Context-Aware processing and Communication Gateway'', Department of Electrical and Computer Engineering, Waterloo, ON N2L 3G1, Canada.

[3] Apoorv saxena, PHY LAYER: IEEE802.11p available at https://apoorvsaxena4.wordpress.com/2015/06/07/phy-layer-ieee-802-11p/., posted on 7 June 2015.

[4] Ali Grami, "Introduction to Digital Communications'', 2016.

[5] Steven W.Smith, Ph.D., "The Scientist and Engineer's guide to Digital Signal Processing'', chapter 6, Second Edition, California Technical Publishing, San Diego, California, 1999.

[6] Sneha H.L, "Basic Signal Operations in DSP: Time shifting, Time Scaling, and Time Reversal'', available at https://www.allaboutcircuits.com/technical-articles/basic-signal-operations-in-dsp-time-shifting-time-scaling-and-time-reversal/, Posted on May 10, 2017.

[7] Gaurang Naik, Biplav Choudhury, Jung-Min Park, "IEEE 802.11bd & 5G NR V2x: Evolution of Radio access technologies for V2x Communications'', Published on May 27, 2019, date of current version June 10, 2019.

[8] Song Gao, Alvin Lim, David Bevly, "An empirical study of DSRC V2V performance in truck platooning scenarios'', Digital Communications and Networks, Volume 2, Issue 4, November 2016, Pages 233-244.

[9] Imad Jawhar, Nader Mohamed, Hafsa Usmani, "An Overview of Inter-Vehicular Communication Systems, Protocols, and Middleware'', Journal of Networks, Vol. 8, NO. 12, December 2013.

[10] Waqar Anwar, Norman Franchi, and Gerhard Fettweis, "Physical layer evaluation of V2x Communications Technologies for 5G NR-V2x, LTE-V2x, IEEE 802.11bd, and IEEE 802.11p'', Vodafone Chair Mobile Communications Systems, Technische Universitat Dresden, Germany, IEEE 90th Vehicular Technology Conference, Honolulu, Hawaii, USA.

[11] Waqar Anwar, Andreas TraBl, Norman Franchi, Gerhard Fettweis, "On the Reliability of NR-V2x and IEEE 802.11bd ", Vodafone Chair Mobile Communications Systems, Technische Universität Dresden, Germany, IEEE 30th Annual International conference Symposium on Personal, Indoor, and Mobile radio communications, Istanbul, Turkey, September 2019.

[12] Andreas Festag, "Standards for vehicular communication from IEEE 802.11p to 5G'', Vodafone Mobile communications, Germany, Published on September 29, 2015.

[13] Molisch, 2011. Wireless Communications, Second Edition, Wiley-IEEE Press.

[14] Carl Gustafson, Kim Mahler, David Bolin, Fredrik Tufesson, "THE COST IRACON Geometry based stochastic Channel model for Vehicle-to-Vehicle Communication in Intersections'', Fraunhofer Heinrich Hertz Institute, Berlin, Germany Mathematical Sciences, Chalmers University of Technology, Gothenburg, Sweden Lund University, Dept. of Electrical and Information Technology, Lund, Sweden.

[15] Loyka, Sergey Kouki, Ammar, "Using Two Ray Multipath Model for Microwave Link Budget Analysis'', IEEE Antennas and Propagation Magazine. 43(5): 31-36, published in October 2001.

[16] Abramowitz, Milton, Stegun, Irene A, "Handbook of mathematical functions with formulas, graphs, mathematical tables'', 1965.

[17] Yochay Lustmann, Danna Porrat, "Indoor channel spectral statistics, K-Factor and Reverberation Distance'', 2010.

[18]   MathWorks.   [Online]   Available   at
     https://se.mathworks.com/help/comm/ref/doppler.html

[19] M. Kahn, "IEEE 802.11 Regulatory SC DSRC Coexistence Tiger Team
     V2V Radio Channel Models ", December 2014.

[20] MathWorks.   [Online]   Available   at
     https://se.mathworks.com/help/comm/ug/fading-channels.html.

[21] Pätzold, Matthias, Cheng-Xiang Wang, and Bjorn Olav Hogstand. "Two
     New Sum-of-Sinusoids-Based Methods for the Efficient Generation of
     Multiple   Uncorrelated   Rayleigh   Fading   Waveforms".   IEEE
     Transactions on Wireless Communications. Vol. 8, Number 6, 2009, pp.
     3122–3131.

[22]   Oestges,   Claude,   and   Bruno   Clerckx. "MIMO   Wireless
     Communications: From Real-World Propagation to Space-Time Code
     Design''. 1st edition. Boston, MA: Elsevier, 2007.

[23] ublox.   [Online]   Available   at   https://github.com/u-blox/ubx-
     V2x/tree/ngv.

[24] Kenzi Meyer, Ece Erdogmus, George Morcous, Mary Naughtin, "Use
     of Ground Penetrating Radar for Accurate Concrete Thickness
     Measurements'', Architectural Engineering Conference, September
     2008.

[25] Payam Vosoughi, Peter Taylor, Halil Ceylan, "Impacts of Internal
     Curing on the performance of Concrete Materials in the Laboratory and
     the Fields'', November 2017.

[26] I. Tan, W. Tang, K. Laberteaux and A. Bahai, "Measurement and
     Analysis of Wireless Channel Impairments in DSRC Vehicular
     Communications", IEEE International Conference on Communications,
     Beijing, 2008, pp. 4882-4888.

[27] Holger Rosier, Florian Richert, "The details of V2x communication",
     October 2019 (source: Intelligent-mobility-experience.com).

[28] Reza Azimi, Gaurav Bhatia, Ragunathan Rajkumar, "Vehicular
     networks for Collision Avoidance at intersections'', Society for

Automotive Engineers (SAE) World Congress, April 2011, Detroit, MI, USA.

[29] Mrs.Vaishali D Khairnar, Dr. S.N. Pradhan, "V2V Communication Survey - Wireless Technology", Research scholar, Professor, Institute of Technology, Nirma University, Posted in March 2014.

[30] Ismail Buyuksaliha, Serdar Bayburta, Gurcan Buyuksaliha, A.P. Baskaracaa, Hairi Karimb and Alias Abdul Rahmanb, "3D MODELLING AND VISUALIZATION BASED ON THE UNITY GAME ENGINE – ADVANTAGES AND CHALLENGES".

List of Figures

List of Tables

List of Acronyms

Avg	Average
AWGN	Additive White Gaussian Noise
BPSC	bits per modulation symbol
BPSK	Binary Phase Shift Keying
Cbps	Coded bits per subcarrier
CDMA	Code Division Multiple Access
CMOS	Complementary Metal Oxide Semiconductor
CDAI	Collision Detection Algorithm for Intersections
CP	Cyclic prefix
CRC	Cyclic Redundancy Check
CSMA	Carrier Sense Multiple Access
CSV	Comma Separated Values
Dbps	Decoded bits per subcarrier
DSRC	Dedicated Short Range Communication
DCM	Data Communication module
DFT	Discrete Fourier Transform
Eff	Efficiency factor
FIT	Finite Impulse response
GSM	Global System for Mobile Communications
LOS	Line Of Sight
LDPC	Low Density Parity Check
LTH	Lund Tekniska Hogskola
MCS	Modulation and Coding Scheme
MPC	Multipath Components
MIMO	Multiple Input Multiple Output
NG-V2X	Next Generation V2X
NLOS	Non Line Of Sight
OFDM	Orthogonal Frequency Division Multiplexing
P	Reflection point
PDA	Personal Digital Assistant
PDA	Personal Digital Assistant
Pdf	Probability density function
PER	Packet Error Rate
PSDU	PLCP Service Data Unit
PLCP	Physical Layer Convergence Protocol
QAM	Quadrature Amplitude Modulation
QPSK	Quadrature Phase Shift Keying

Rx	Receiver
RX_G	Receiver Ground position
SNR	Signal to Noise Ratio
SISO	Single Input Single Output
STBC	Space time block coding
Tx	Transmitter
TX_G	Transmitter ground position
UWB	Ultra-Wide Band Technology
UWB	Ultra-Wide Band Technology
V2X	Vehicle to Everything
WAVE	Wireless Access in Vehicular Environment
WSSUS	Wide Sense Stationary Uncorrelated Scatterers
3D	Three dimensional